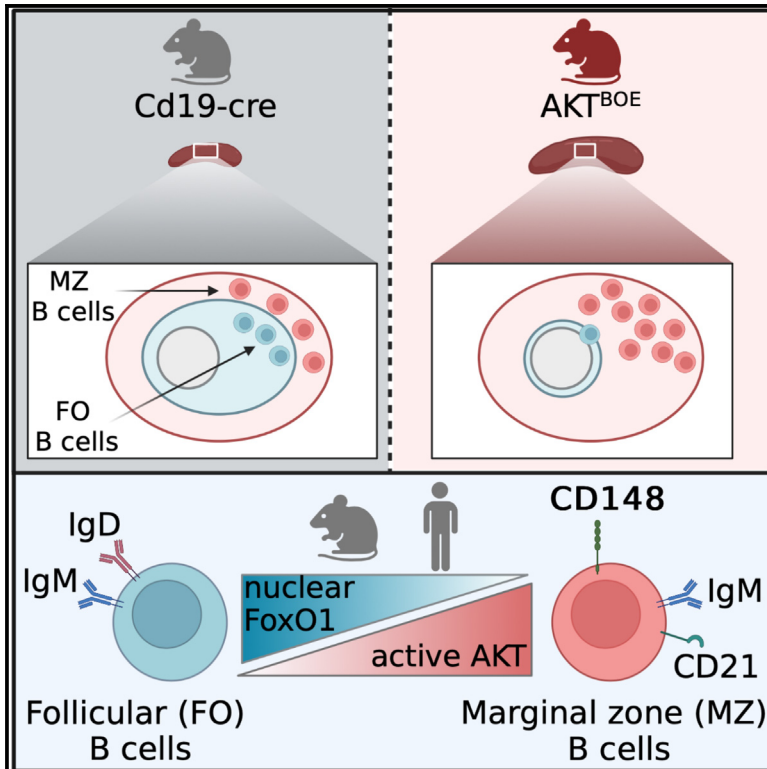


## AKT activity orchestrates marginal zone B cell development in mice and humans

### Graphical abstract



### Authors

Eva-Maria Cox, Mohamed El-Behi, Stefanie Ries, ..., F. Thomas Wunderlich, Nadine Hövelmeyer, Simon Fillatreau

### Correspondence

hoevelme@uni-mainz.de (N.H.),  
simonfillatreau@googlemail.com (S.F.)

### In brief

Cox et al. show that AKT activation biases B cell development toward marginal zone (MZ) B cells with innate functions. CD148 is identified as a receptor indicative of AKT signaling level in B cells, expressed at higher levels in MZ than FO B cells in mice and humans.

### Highlights

- AKT signaling in B cells drives MZ B cell development
- FoxO1 inactivation is necessary for MZ B cell development
- AKT is also distinctively increased in human IgD<sup>+</sup>CD27<sup>+</sup> MZ B cells
- CD148 is expressed at higher levels in MZ B cells than FO B cells in mice and humans



## Article

# AKT activity orchestrates marginal zone B cell development in mice and humans

Eva-Maria Cox,<sup>1</sup> Mohamed El-Behi,<sup>2</sup> Stefanie Ries,<sup>3</sup> Johannes F. Vogt,<sup>1</sup> Vivien Kohlhaas,<sup>4,5,6,7,8</sup> Thomas Michna,<sup>9</sup> Benoît Manfroi,<sup>2</sup> Mona Al-Maarri,<sup>4,5,6,7,8</sup> Florian Wanke,<sup>1</sup> Boaz Tirosh,<sup>10</sup> Corinne Pondarre,<sup>11,12</sup> Harry Lezeau,<sup>11,12</sup> Nir Yogev,<sup>13</sup> Romy Mittenzwei,<sup>1</sup> Marc Descatoire,<sup>14</sup> Sandra Weller,<sup>2</sup> Jean-Claude Weill,<sup>2</sup> Claude-Agnès Reynaud,<sup>2</sup> Pierre Boudinot,<sup>15</sup> Luc Jouneau,<sup>15</sup> Stefan Tenzer,<sup>9,16,17</sup> Ute Distler,<sup>9</sup> Anne Rensing-Ehl,<sup>18</sup> Christoph König,<sup>18,19</sup> Julian Staniek,<sup>20</sup> Marta Rizzi,<sup>20,21,22</sup> Aude Magérous,<sup>23</sup> Frederic Rieux-Laucat,<sup>23</sup> F. Thomas Wunderlich,<sup>4,5,6,7,8</sup> Nadine Hövelmeyer,<sup>1,16,26,27,\*</sup> and Simon Fillatreau<sup>2,24,25,26,\*</sup>

<sup>1</sup>Institute for Molecular Medicine Mainz, University Hospital of Mainz, 55131 Mainz, Germany

<sup>2</sup>Institut Necker Enfants Malades, INSERM U1151-CNRS UMR 8253, 156-160, rue de Vaugirard, 75015 Paris, France

<sup>3</sup>Deutsches Rheuma-Forschungszentrum, a Leibniz Institute, 10117 Berlin, Germany

<sup>4</sup>Max Planck Institute for Metabolism Research Cologne, 50931 Cologne, Germany

<sup>5</sup>Institute for Genetics, University of Cologne, 50931 Cologne, Germany

<sup>6</sup>Cologne Excellence Cluster on Cellular Stress Responses in Aging-associated Diseases (CECAD), 50931 Cologne, Germany

<sup>7</sup>Center for Molecular Medicine Cologne (CMMC), 50931 Cologne, Germany

<sup>8</sup>Center for Endocrinology, Diabetes and Preventive Medicine (CEDP) Cologne, 50931 Cologne, Germany

<sup>9</sup>Institute for Immunology, University Medical Centre of the Johannes-Gutenberg University Mainz, Mainz, Germany

<sup>10</sup>The Hebrew University of Jerusalem, Institute for Drug Research, Jerusalem, Israel

<sup>11</sup>Service de Pédiatrie Générale, Centre de Référence de la Drépanocytose, Centre Intercommunal de Créteil, Créteil, France

<sup>12</sup>Inserm U955, Université Paris XII, Créteil, France

<sup>13</sup>Faculty of Medicine, Department of Dermatology, University of Cologne, 50931 Cologne, Germany

<sup>14</sup>Laboratory of Immune Inherited Disorders, Department of Immunology and Allergology Lausanne Hospital CHUV, Lausanne, Switzerland

<sup>15</sup>Université Paris-Saclay, INRAE, UVSQ, VIM, 78350 Jouy-en-Josas, France

<sup>16</sup>Research Centre for Immunotherapy (FZI), University Medical Center of the Johannes-Gutenberg University Mainz, Mainz, Germany

<sup>17</sup>Helmholtz Institute for Translational Oncology Mainz (HI-TRON Mainz), Mainz, Germany

<sup>18</sup>Institute for Immunodeficiency, Center for Chronic Immunodeficiency, Medical Center-University of Freiburg, Faculty of Medicine, University of Freiburg, Freiburg, Germany

<sup>19</sup>University of Freiburg, Faculty of Biology, Schaenzlestrasse 1, 79104 Freiburg, Germany

<sup>20</sup>Department of Rheumatology and Clinical Immunology, University Medical Center Freiburg, Faculty of Medicine, University of Freiburg, Freiburg, Germany

<sup>21</sup>Center for Chronic Immunodeficiency, Medical Center-University of Freiburg, Faculty of Medicine, University of Freiburg, Freiburg, Germany

<sup>22</sup>Division of Clinical and Experimental Immunology, Institute of Immunology, Center for Pathophysiology, Infectiology and Immunology, Medical University of Vienna, Vienna, Austria

<sup>23</sup>Université Paris Cité, Institut Imagine, Laboratory of Immunogenetics of Pediatric Autoimmune Diseases, INSERM UMR 1163, 75015 Paris, France

<sup>24</sup>Université de Paris Cité, Paris Descartes, Faculté de Médecine, Paris, France

<sup>25</sup>AP-HP, Hôpital Necker Enfants Malades, Paris, France

<sup>26</sup>These authors contributed equally

<sup>27</sup>Lead contact

\*Correspondence: [hoevelme@uni-mainz.de](mailto:hoevelme@uni-mainz.de) (N.H.), [simonfillatreau@googlemail.com](mailto:simonfillatreau@googlemail.com) (S.F.)

<https://doi.org/10.1016/j.celrep.2023.112378>

## SUMMARY

The signals controlling marginal zone (MZ) and follicular (FO) B cell development remain incompletely understood. Here, we show that AKT orchestrates MZ B cell formation in mice and humans. Genetic models that increase AKT signaling in B cells or abolish its impact on FoxO transcription factors highlight the AKT-FoxO axis as an on-off switch for MZ B cell formation in mice. In humans, splenic immunoglobulin (Ig) D<sup>+</sup>CD27<sup>+</sup> B cells, proposed as an MZ B cell equivalent, display higher AKT signaling than naive IgD<sup>+</sup>CD27<sup>-</sup> and memory IgD<sup>-</sup>CD27<sup>+</sup> B cells and develop in an AKT-dependent manner from their precursors *in vitro*, underlining the conservation of this developmental pathway. Consistently, CD148 is identified as a receptor indicative of the level of AKT signaling in B cells, expressed at a higher level in MZ B cells than FO B cells in mice as well as humans.



## INTRODUCTION

B cells can mount antibody responses against virtually any antigen. Depending on its biochemical nature, follicular (FO) or marginal zone (MZ) B cells are differentially involved, with a major contribution of MZ B cells for polysaccharide antigens.<sup>1</sup> MZ B cells also differ from FO B cells by their higher innate functions.<sup>2,3</sup> The relative abundance of MZ and FO B cells thus modulates the immune competence of the host.

The development of immature B cells into either FO or MZ B cells occurs after their egress from bone marrow.<sup>4,5</sup> This cell fate decision is guided by signals transmitted in B cells via NOTCH2, the B cell receptor for antigen (BCR), and B-cell activating factor (BAFF) receptors.<sup>6,7</sup> Mice lacking *Notch2* in B cells lack MZ B cells,<sup>8</sup> and the expression of a constitutive active NOTCH2 in B cells is sufficient to increase the proportion of MZ B cells from 10% to 60%–80%.<sup>9</sup> An increase in MZ B cells is also observed in mice with the gain-of-function mutation in *NOTCH2* associated with the Hajdu-Cheney syndrome.<sup>10</sup> Of note, mature FO B cells can also be converted into MZ B cells upon the genetic activation of NOTCH2 signaling, underlining the plasticity of these cell states.<sup>11</sup> The NOTCH2 ligand Delta-like 1 (DLL1), which is required for MZ B cell development,<sup>12</sup> is found in mice spleen in the MZ on fenestrated venules of endothelial niches,<sup>13,14</sup> and on epithelial cells in B cell follicles.<sup>14</sup> Its presence in the human splenic MZ has also been documented.<sup>15</sup> The instruction of MZ B cell commitment by NOTCH2 involves its canonical signaling because the deletion of the recombination signal binding protein for immunoglobulin kappa J region (RBPJ) gene in B cells results in the lack of MZ B cells.<sup>16</sup> However, NOTCH2 additionally activates Jun N-terminal kinase (JNK), extracellular signal-regulated kinases (ERKs), and the serine/threonine kinase AKT (also known as PKB).<sup>9,10,17</sup> These signaling pathways are also activated via the BCR, which influences MZ B cell differentiation,<sup>18,19</sup> suggesting that they might contribute to MZ B cell formation.<sup>20</sup> The major BCR co-receptor CD19 is required for the formation of these cells.<sup>21–23</sup> A key function of CD19 is to stimulate phosphoinositide 3-kinase (PI3K) signaling because loss-of-function mutations in the PI3K isoform p110 $\delta$  decreases MZ B cell numbers.<sup>24</sup> Downstream of PI3K are Bruton's tyrosine kinase (BTK) and AKT. The loss of BTK reduces total splenic B cell number, but all subsets persist.<sup>25</sup> The co-deletion of *Akt1* and *Akt2* in mouse B cells seems to have a stronger effect on MZ B cell development, which is then almost completely abrogated; however, this gene deletion also reduces the number of FO B cells.<sup>26</sup> These data indicate that AKT contributes to MZ B cell formation but leave its quantitative role unknown.

The deletion of genes encoding for AKT signaling inhibitors modestly increased MZ B cell formation. The deletion of *Pten* raised MZ B cells abundance, yet most B cells retained an FO phenotype.<sup>27,28</sup> A similar phenotype was observed in mice with a B cell-specific deletion of the transcription factor Forkhead Box O1 (FoxO1), which is excluded from the nucleus and degraded upon phosphorylation by AKT.<sup>28,29</sup> Thus, increasing AKT signaling does not seem to have a major effect on B cell development. However, the employed approaches were indirect. PTEN has other activities, modulating the func-

tion of other kinases<sup>30,31</sup> and acting as a scaffolding protein.<sup>31,32</sup> The loss of PTEN is therefore not equivalent to AKT overactivity.<sup>31</sup> Deletion of *FoxO1* gene is also not a perfect mimic of increased AKT activity because AKT phosphorylates more than 300 substrates.<sup>33</sup>

To our knowledge, no study has addressed directly how increasing AKT activity in B cells affects their commitment toward MZ B cells, even though NOTCH2, BCR, and BAFF-R,<sup>34</sup> which all contribute to MZ B cell formation, converge on AKT. Here, we directly addressed the role of AKT in MZ B cell formation using genetic, transcriptomic, and cytometric approaches.

## RESULTS

### AKT signaling in B cells drives MZ B cell development in mice

We studied the role of AKT in B cells using a mouse harboring in the *Rosa26* locus a sequence (preceded by a loxP-flanked stop cassette) coding for a mutant AKT-1 carrying an N-terminal myristylation tag.<sup>35</sup> *Cd19*-cre-mediated recombination of the stop cassette leads to B cell-specific *Akt-C* activity (AKT<sup>BOE</sup> mice) (Figure S1A).<sup>35</sup> The myristylation tag localizes the mutant AKT-1 to the plasma membrane where it is phosphorylated and activated. Western blot analyses of B cells from AKT<sup>BOE</sup> and control mice confirmed the increased phosphorylation of AKT at Thr308 and Ser473 (Figure S1B). AKT<sup>BOE</sup> mice were born at expected mendelian ratio, and did not develop leukemia or lymphoma, in agreement with previous findings.<sup>35</sup>

Flow cytometry analysis revealed normal B cell development in the bone marrow of AKT<sup>BOE</sup> mice (Figure S1C). However, at 6 weeks of age, AKT<sup>BOE</sup> mice showed increased spleen size and cell numbers (Figure 1A), while the ratio of B and T cells was not changed (Figure 1B). Thus, total numbers of B cells and T cells (Figure 1B), as well as myeloid cells and natural killer (NK) cells, were all increased (Figure S1D). Remarkably, the splenic B cell compartment of AKT<sup>BOE</sup> mice was composed almost exclusively of CD21<sup>hi</sup>CD23<sup>lo</sup> MZ-like B cells, whereas CD21<sup>int</sup>CD23<sup>hi</sup> FO B cells were nearly absent (Figure 1C). CD21<sup>hi</sup>CD23<sup>lo</sup> B cells displayed a distinctive CD21<sup>hi</sup>CD1d<sup>hi</sup> cell surface phenotype (Figure 1D), expressed high levels of immunoglobulin (Ig) M and low levels of IgD (Figure 1E), and accumulated around metallophilic macrophages (Figure 1F), indicating a phenotype and localization typical of MZ B cells. The spleen of AKT<sup>BOE</sup> mice displayed normally segregated B cell follicles and T cell zones (Figure 1G). AKT<sup>BOE</sup> mice also displayed an increased abundance of CD21<sup>−</sup>CD23<sup>−</sup> double-negative (DN) B cells (Figure 1C), which included CD43<sup>+</sup>CD5<sup>+</sup>, CD43<sup>+</sup>CD5<sup>−</sup>, CD43<sup>−</sup>CD5<sup>−</sup> B cells and plasmacytes (Figure S1E).

To determine whether the accumulation of MZ-like B cells seen in AKT<sup>BOE</sup> mice was due to increased proliferation, mice were fed with 5-bromo-2'-deoxyuridine (BrdU) for 7 days and then analyzed by flow cytometry. The percentage of BrdU<sup>+</sup> B cells was lower in spleen and mesenteric lymph nodes (mLN) of AKT<sup>BOE</sup> mice compared with controls (Figure S1F), showing that the MZ-like B cell excess was not related to proliferation. Remarkably, 3-week-old AKT<sup>BOE</sup> mice already displayed an overwhelming abundance of CD21<sup>hi</sup>CD23<sup>lo</sup> MZ-like B cells, while these cells were rare (<2%) in controls at this age

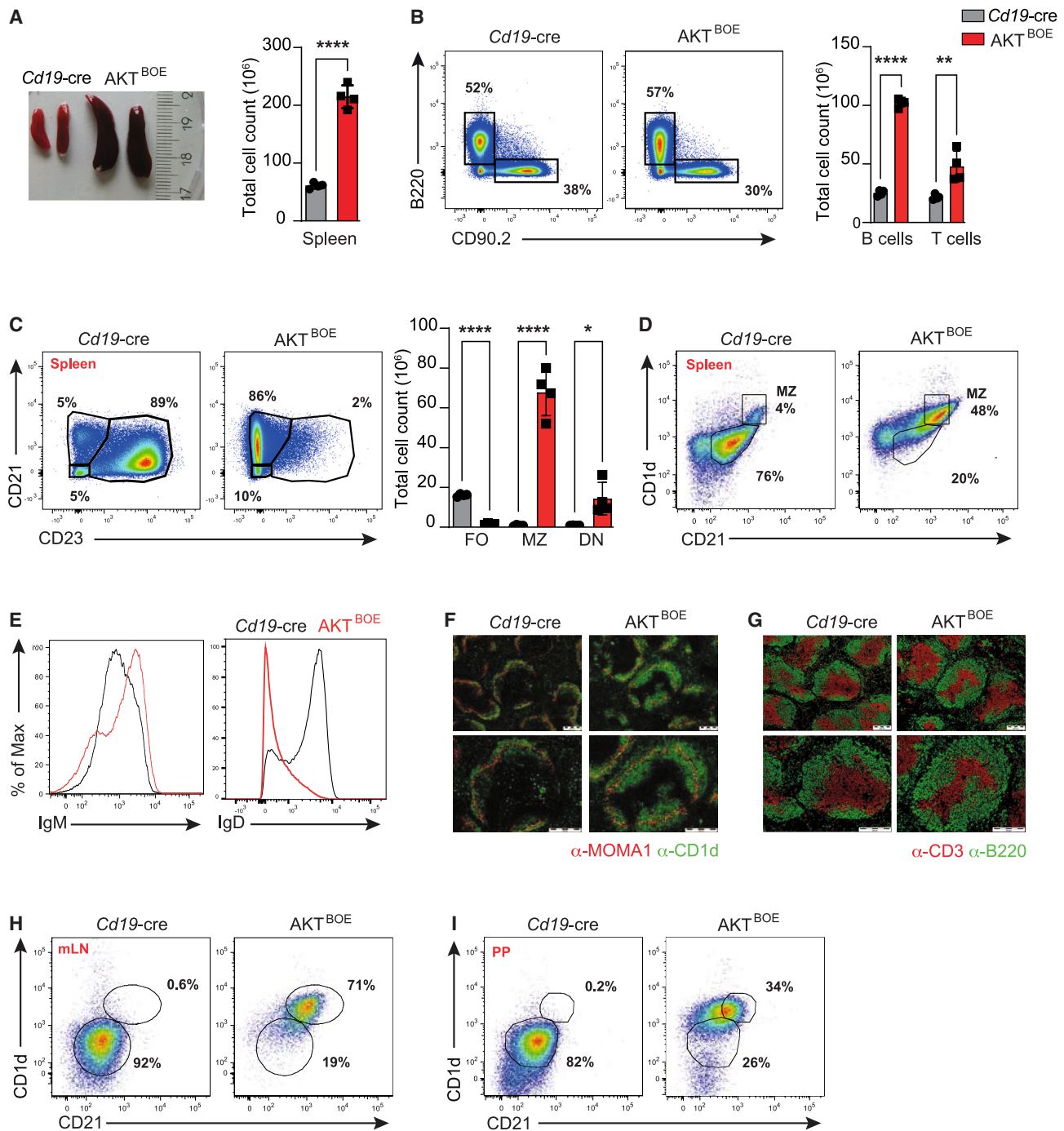


**Figure 1. AKT signaling in B cells drives MZ B cell development in mice**

(A) Splens from *AKT<sup>BOE</sup>* and *Cd19-cre* control mice (left). Ruler indicates the size of organ (centimeters). Picture is representative for at least 10 mice/genotype. Total cell count of splenocytes (right).

(B) Representative flow cytometry analysis of CD90.2<sup>+</sup> T cells and B220<sup>+</sup> B cells from *AKT<sup>BOE</sup>* and control mice (left). Numbers in plots represent the percentage of B and T cells. Total cell count of splenic B220<sup>+</sup> B and CD90.2<sup>+</sup> T cells (right).

(C) Flow cytometry analysis of CD21 and CD23 expression on live splenic CD19<sup>+</sup> lymphocytes (left). Numbers represent the percentage of CD23<sup>low</sup>CD21<sup>high</sup> MZ and CD23<sup>+</sup>CD21<sup>+</sup> FO and CD21<sup>-</sup>CD23<sup>-</sup> double-negative (DN) B cells. Total cell numbers of follicular (FO), marginal zone (MZ), and DN B cells (right).

(D) Flow cytometry analysis of CD1d and CD21 expression on live splenic CD19<sup>+</sup> lymphocytes.

(E) Representative histograms of IgM and IgD surface staining on splenic CD19<sup>+</sup> B cells.

(legend continued on next page)

(Figure S1G), suggesting that AKT switched B cell development toward the MZ fate. B cells from AKT<sup>BOE</sup> mice displayed an increased survival compared with controls (Figure S1H), which is likely involved in the B cell expansion in these mice (Figure 1B).

To assess whether this MZ-like B cell accumulation was restricted to spleen, we next examined other secondary lymphoid tissues. As shown in Figures 1H and 1I, MZ-like B cells were the dominant subset in mLN and Peyer's patches of AKT<sup>BOE</sup> mice, while, as expected, they were absent in these tissues in control mice. In peritoneal cavity, B1a, B1b, and B2 cells were increased in AKT<sup>BOE</sup> mice compared with controls (Figure S1I).

Thus, increasing AKT activity is sufficient to drive B cell development toward MZ-like B cells, which are then the main B cell subset in spleen and LN.

### Role of AKT in the transcriptional program of MZ B cells

We next analyzed AKT contribution to MZ B cell transcriptional program by comparing the transcriptomes of FO B cells from control mice, MZ B cells from control mice, and MZ-like B cells from AKT<sup>BOE</sup> mice.

MZ and FO B cells from controls differed in the expression of 1206 genes (1,439 Affymetrix probes) (Table S1), including 71 transcriptional regulators (adjusted  $p < 0.01$ ) (Table S2). To identify whether AKT might be implicated in these differences, we extracted the list of genes differentially expressed between both (1) MZ B cells and FO B cells from control mice (Table S1) and (2) MZ-like B cells from AKT<sup>BOE</sup> mice and FO B cells from control mice (Table S3). We found that 782 out of 1,206 genes (65%) (905 out of 1,439 Affy IDs) differentially expressed between control FO and MZ B cells were modulated by AKT (Figure 2A; Table S4). These genes contained 45 transcriptional regulators, including factors that control MZ B cell development such as *Ikaros* and *Hes1* (higher expression in MZ B cells), as well as *Irf8*, *Klf2*, *Fli1*, *Bach2*, and *Bcl6* (higher expression in FO B cells) (Figure 2B).<sup>36–39</sup> Several pathways and Gene Ontology (GO) terms were shared between MZ-like B cells from AKT<sup>BOE</sup> and MZ B cells from control mice compared with FO B cells (Table S5). In contrast, few pathways and GO terms were present in control MZ B cells but not in MZ-like B cells from AKT<sup>BOE</sup> mice (compared with FO B cells) (Table S6). These data suggest that AKT plays a prominent role in the MZ B cell transcriptional program.

Differential expression of *Hes1* suggested that AKT induced NOTCH2 activation. NOTCH2 target genes were differentially expressed between MZ-like B cells from AKT<sup>BOE</sup> mice and control FO B cells, including *Atxn1*, *Maml1*, *Hes1*, *Adam17*, and *Dtx1* (Figures 2C and S2A). NOTCH2 activation implicates ADAM28 and ADAM10,<sup>40</sup> whose expression involves TAO3, which is required for MZ B cell development.<sup>40</sup> *Taok3* expression was

higher in MZ-like B cells from AKT<sup>BOE</sup> (Table S3) and MZ B cells from control mice (Table S1) compared with FO B cells. ADAM17 also contributes to MZ B cell formation,<sup>41</sup> and *Adam17* expression was higher in the two MZ B cell fractions than in FO B cells (Tables S1 and S3). Finally, western blot analysis showed that B cells from AKT<sup>BOE</sup> mice had increased NOTCH2 expression and processing compared with control B cells (Figure 2D). These data corroborate the notion that AKT signaling leads to NOTCH2 activation.

We expected MZ-like B cells from AKT<sup>BOE</sup> mice to differ from control MZ B cells. We looked for transcriptional regulators differentially expressed between control MZ and FO B cells but not modulated by AKT hyperactivity (Figure S2B). This identified *Myc*, a gene essential for B cell proliferation and differentiation into antibody-secreting cells as well as germinal centers.<sup>42–44</sup> AKT hyperactivity also failed to upregulate *Ahr*, which contributes to MZ B cells homeostasis.<sup>45</sup> To gain a global appreciation of the processes differentially active in MZ-like B cells from AKT<sup>BOE</sup> mice compared with controls, we performed pathway analyses on genes differentially expressed between MZ-like B cells from AKT<sup>BOE</sup> mice and FO B cells from controls, which were not differentially expressed between control MZ and FO B cells (Tables S4 and S7). This highlighted pathways and GO terms related to mitochondria (Table S7). MZ-like B cells from AKT<sup>BOE</sup> mice might thus differ from control MZ B cells by their mitochondria activity.

Collectively, these analyses show that a large part of the transcriptional program distinguishing MZ from FO B cells is recapitulated in cells with increased AKT signaling, including transcriptional regulators known to control MZ B cell formation. In addition, increased AKT signaling promotes NOTCH2 activity. This molecular analysis underlines the role of AKT in MZ B cell development.

### Enforced AKT activity overcomes Cd19 deficiency for MZ B cell accumulation

AKT is activated downstream of BCR and CD19 via PI3K signaling.<sup>46</sup> To evaluate if other effector downstream of CD19 aside AKT was necessary for MZ B cell formation,<sup>47,48</sup> we analyzed MZ B cell development in AKT<sup>BOE</sup>CD19<sup>KO</sup> mice obtained by crossing mice homozygous for the *Cd19*-cre knockin allele, which lack both CD19 protein (CD19<sup>KO</sup>) and MZ B cells,<sup>21–23</sup> with AKT<sup>BOE</sup> mice.

AKT<sup>BOE</sup>CD19<sup>KO</sup> mice displayed increased spleen size and cell numbers compared with CD19<sup>KO</sup> controls (Figure 3A). The splenic B cell compartment showed an almost complete shift toward MZ-like B cells having a CD21<sup>hi</sup>CD23<sup>lo</sup> and CD21<sup>hi</sup>CD1d<sup>hi</sup> phenotype, as observed in AKT<sup>BOE</sup> mice (Figures 3B–3D). The histological examination of spleens using anti-CD1d and anti-MOMA1 antibodies indicated that CD1d<sup>hi</sup> B cells were localized

(F) Immunofluorescence analysis of spleens from AKT<sup>BOE</sup> and *Cd19*-cre control animals stained for MZ B cells (CD1d<sup>+</sup>, green) and metallophilic macrophages (MOMA-1<sup>+</sup>, red). Scale bar, 200  $\mu$ m; magnification,  $\times 20$ .

(G) Immunofluorescence analysis of spleens stained for B cells (B220<sup>+</sup>, green) and T cells (CD3<sup>+</sup>, red). Scale bar, 200  $\mu$ m; magnification,  $\times 20$ .

(H and I) Flow cytometry plots showing CD1d and CD21 expression on live CD19<sup>+</sup> lymphocytes from mLN (H) and PP (I). Analyses performed using 8–12-week-old *Cd19*-cre and AKT<sup>BOE</sup> mice. Data are representative of at least three independent experiments with  $n = 4$  mice per experiment per genotype. Bar graphs show means  $\pm$  SDs and single values. Statistical significance was calculated using two-tailed unpaired t test with Holm-Sidak correction for multiple comparison; \* $p < 0.05$ , \*\* $p < 0.01$ , \*\*\*\* $p < 0.0001$ . See also Figure S1.

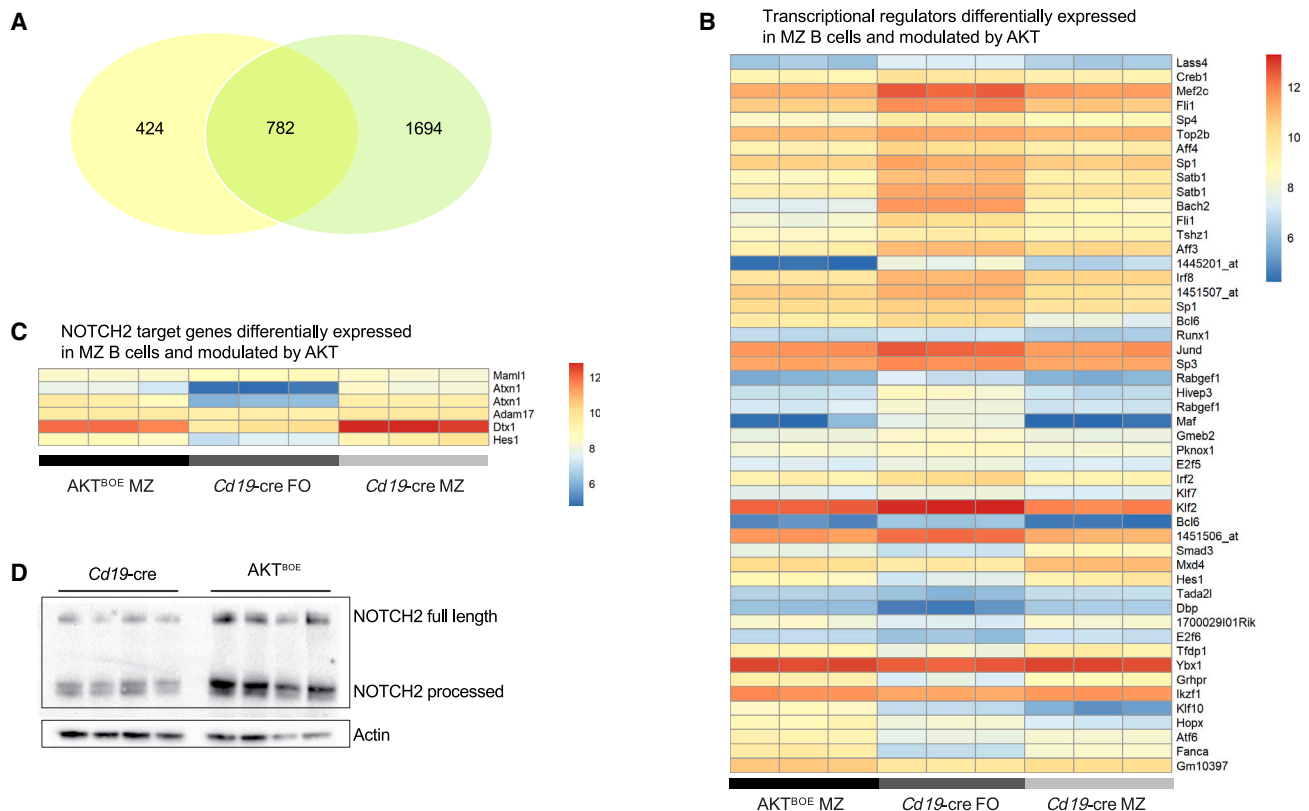


**Figure 2. AKT contribution to MZ B cells transcriptional program**

(A) Venn diagram with yellow area indicating the number of genes differentially expressed between MZ B cells and FO B cells from control mice, the green area showing the number of genes differentially expressed between MZ B cells from AKT<sup>BOE</sup> mice and FO B cells from control mice, and their intersection. (B) Normalized gene expression levels in MZ B cells from AKT<sup>BOE</sup> mice, FO B cells from *Cd19-cre* mice, and MZ B cells from *Cd19-cre* mice for transcriptional regulators differentially expressed between (i) MZ B cells and FO B cells from *Cd19-cre* mice and (ii) MZ B cells from AKT<sup>BOE</sup> mice versus FO B cells from *Cd19-cre* mice. (C) Normalized gene expression levels for NOTCH2 target genes differentially expressed between (i) MZ versus FO B cells from *Cd19-cre* mice and (ii) MZ B cells from AKT<sup>BOE</sup> mice versus FO B cells from *Cd19-cre* mice. (D) Western blot showing full-length and processed NOTCH2 in B cells from *Cd19-cre* and AKT<sup>BOE</sup> mice. Data show four mice per genotype; representative of three independent experiments. (A–C) Microarrays in triplicate. (B and C) Expression amounts normalized using GCRMA are shown (Log2 transformed). See also Figure S2.

around the MZ in AKT<sup>BOE</sup>CD19<sup>KO</sup> mice, while these B cells were absent in CD19<sup>KO</sup> mice (Figure 3E). This B cell phenotype was associated with an increased abundance of DN B cells (Figure 3D), CD4 T cells, CD8 T cells, myeloid cells, and NK cells in spleen (Figures S3A–S3C), as well as B1a, B1b, and B2 cells in PerC (Figure S3D).

We conclude that enhancing AKT activity is sufficient to restore MZ-like B cell development in CD19<sup>KO</sup> mice. Thus, CD19 and PI3K do not seem to deliver any indispensable signal for MZ B cell development beyond those controlled by AKT.

### FoxO1 inactivation is necessary for MZ B cell development

AKT has more than 300 substrates,<sup>33</sup> suggesting that it might contribute to MZ B cells in multiple ways. A relevant substrate is FoxO1 because the deletion of its gene modestly increases MZ B cell development.<sup>28</sup> We examined the role of FoxO1 inactivation by AKT for MZ B cell formation.

As expected, B cells from AKT<sup>BOE</sup> mice displayed a lower FoxO1 level than control B cells (Figure S3E). To assess whether FoxO inhibition by AKT was central to MZ B cell development, we crossed mice expressing (upon the deletion of a LoxP-flanked STOP cassette) a transgenic FoxO1 mutant insensitive to the inhibitory effect of AKT due to mutations at three specific phosphorylation sites (FoxO1<sup>ADA</sup> mice)<sup>49</sup> with *Cd19-cre* mice, to restrict this genetic modification to B cells. Mice with higher FoxO1 activity in B cells had spleens of normal size compared with *Cd19-cre* mice (Figure 3F) but almost completely lacked MZ B cells (Figure 3G).

To assess whether increasing AKT signaling could overcome the effect of the mutant FoxO1, we crossed AKT<sup>BOE</sup> mice and FoxO1<sup>ADA</sup> mice. FoxO1<sup>ADA</sup>AKT<sup>BOE</sup> mice displayed an increased spleen size like AKT<sup>BOE</sup> mice (Figure 3F), indicating that this AKT-dependent growth effect was independent of FoxO1 phosphorylation by AKT. However, FoxO1<sup>ADA</sup>AKT<sup>BOE</sup> mice mostly had FO B cells (Figure 3G). The relative abundance of MZ and FO B cells

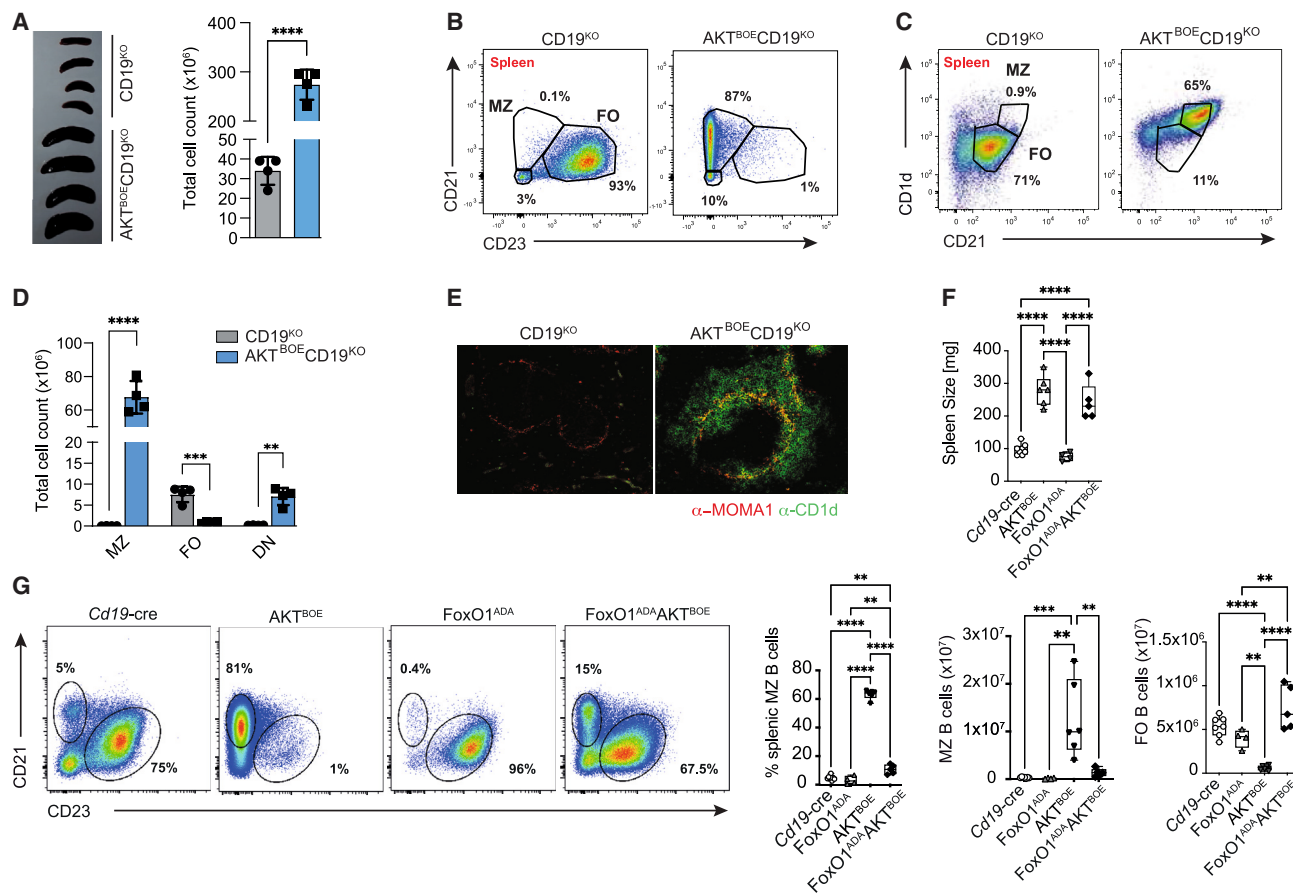


**Figure 3. Enforced AKT activity overcomes *Cd19* deficiency for MZ B cell development**

(A) Representative pictures of spleens from AKT<sup>BOE</sup>CD19<sup>KO</sup> and CD19<sup>KO</sup> mice, and total count of splenocytes.

(B) Flow cytometry analysis of CD21 and CD23 expression on live splenic B cells from CD19<sup>KO</sup> and AKT<sup>BOE</sup>CD19<sup>KO</sup> mice.

(C) Flow cytometry analysis of CD1d and CD21 on live splenic B lymphocytes.

(D) Total splenic numbers of MZ, FO, and CD21<sup>+</sup>CD23<sup>-</sup>DN B cells.

(E) Representative immunofluorescence analysis of spleens stained for MZ B cells (CD1d<sup>+</sup>, green) and metallophilic macrophages (MOMA-1<sup>+</sup>, red). Magnification ×20.

(F) Spleen weight measured in mg (8-week-old mice).

(G) Flow cytometry analysis of CD21 and CD23 expression on live splenic B cells from *Cd19-cre*, AKT<sup>BOE</sup>, FoxO1<sup>ADA</sup>, and FoxO1<sup>ADA</sup>AKT<sup>BOE</sup> mice (left). Percentage and total cell numbers of MZ B cells, and total cell numbers of FO B cells (right). Analyses performed in 8- to 12-week-old mice. Data representative of at least three independent experiments with n = 3–4 mice per genotype per experiment. Bar graphs show means ± SD and single values; \*\*p < 0.01, \*\*\*p < 0.001, \*\*\*\*p < 0.0001, two-tailed unpaired t test (A) with Holm-Sidak correction for multiple comparison (D), and one-way ANOVA (F and G). See also Figure S3.

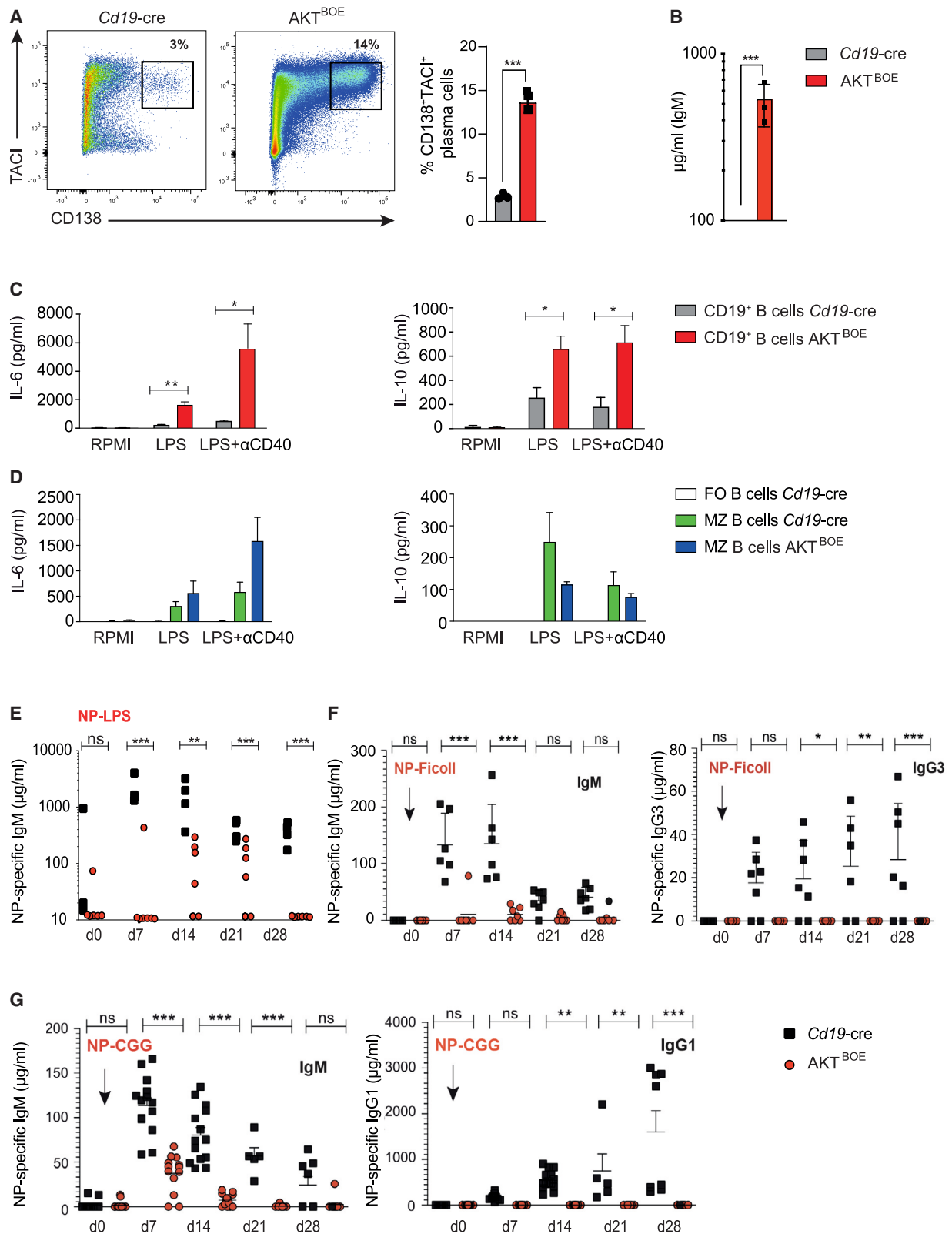
was thus not strictly correlated with the increased spleen size. This underlines the role of the AKT-FoxO1 axis in MZ B cell differentiation.

We conclude that the ratio between AKT and FoxO1 operates as a switch for MZ B cell development, which can, depending on its level, drive the almost exclusive production of MZ-like B cells or completely block this process.

### MZ-like B cells from AKT<sup>BOE</sup> mice have innate functions

MZ B cells functionally differ from FO B cells by their stronger innate response to Toll-like receptor (TLR) agonists, which leads to the generation of antibody-secreting cells and cytokine production.<sup>2</sup> We thus compared the response of B cells from AKT<sup>BOE</sup> and control mice to lipopolysaccharide (LPS) *in vitro*.

B cells from AKT<sup>BOE</sup> mice displayed a stronger differentiation into plasmablasts expressing CD138 and transmembrane activator and CAML interactor (TACI) than control B cells upon LPS stimulation (Figure 4A), which was associated with higher amounts of secreted IgM in culture supernatants (Figure 4B). B cells from AKT<sup>BOE</sup> mice also produced more interleukin (IL)-6 and IL-10 than control B cells upon TLR stimulation (Figure 4C). Repeating this experiment using purified MZ-like B cells from AKT<sup>BOE</sup> and MZ B cells from control mice indicated that MZ-like B cells from AKT<sup>BOE</sup> mice produced slightly more IL-6 and less IL-10 than control MZ B cells upon LPS or LPS + αCD40 stimulation, yet the differences were not statistically significant. In contrast, FO B cells failed to produce these cytokines (Figure 4D). Collectively, these data indicate that B



(legend on next page)

cells from AKT<sup>BOE</sup> mice can make functional innate responses to TLR stimulation, which is a distinctive feature of MZ B cells. Thus, AKT signaling can drive the development of innate MZ-like B cells.

### B cells from AKT<sup>BOE</sup> mice display impaired antibody responses *in vivo*

A distinctive feature of MZ B cells is their capacity to make antibody responses to T cell-independent antigens *in vivo*. To analyze this capacity for AKT<sup>BOE</sup> mice, we immunized these mice with NP-LPS or NP-Ficoll, which are classical T cell-independent type 1 and type 2 antigens, respectively, or NP-CGG, a T cell-dependent antigen. An antigen-specific antibody response could be detected in most AKT<sup>BOE</sup> mice 2–3 weeks after immunization with NP-LPS, although at lower levels than in controls (Figure 4E). In contrast, the response to NP-Ficoll was largely defective in these mice (Figure 4F). They also developed a weaker IgM response to NP-CGG, and a lack of IgG to that antigen (Figure 4G), which was associated with the absence of germinal centers in spleen (Figure S4).

### B cells from AKT<sup>BOE</sup> mice have altered BCR signaling

The normal innate response of MZ-like B cells from AKT<sup>BOE</sup> mice and their defective antigen-specific activation *in vivo* suggested that their BCR signaling was altered. B cells from AKT<sup>BOE</sup> mice failed almost completely to proliferate upon anti-IgM stimulation, compared with control B cells (Figure 5A). In contrast, they proliferated in response to TLR agonists (Figure 5A), suggesting an alteration of BCR function rather than a general defect in cell proliferation. We thus examined BCR signaling in these cells. AKT<sup>BOE</sup> B cells displayed a lack of calcium response upon BCR engagement (Figure 5B). The analysis of global tyrosine phosphorylation upon BCR engagement confirmed the alteration of this signaling, with the increased tyrosine phosphorylation of a large protein (>160 kDa) already at 1-min post-BCR engagement, and the decreased tyrosine phosphorylation of smaller proteins (50–80 kDa) in B cells from AKT<sup>BOE</sup> mice compared with controls (Figure 5C). A specific investigation of BCR signaling pathway molecules indicated that CD79 phosphorylation was normally induced in B cells from AKT<sup>BOE</sup> mice (Figure 5D), whereas the phosphorylation of CD19, SYK, and BTK was reduced (Figures 5E–5G).

To gain an unbiased view of BCR signaling, we performed a comparative phospho-proteomic analysis of B cells from AKT<sup>BOE</sup> and control mice at steady state and after activation with anti-IgM (Figure S5A; Tables S8, S9, and S10). B cells from AKT<sup>BOE</sup> mice displayed the differential phosphorylation of 533 peptides upon IgM stimulation compared with their unstimulated counterpart (Figure S5B). About one-third of these differentially phosphorylated peptides showed a similar response in control B cells (Figure S5B), indicating that the response to IgM was not completely erased in B cells from AKT<sup>BOE</sup> mice. The analysis of the pathways linked to these shared changes indicated an enrichment in metabolism as well as RNA transcription and processing pathways (Table S11). In keeping with this, similarly phosphorylated proteins included AGFG1, which is involved in RNA transport<sup>50</sup>; LARP1, which regulates the translation of specific mRNA downstream of mTORC1<sup>51</sup>; and the RNA-binding protein RBM14<sup>52</sup> (Figure S5C). The phospho-proteome of anti-IgM-stimulated AKT<sup>BOE</sup> B cells differed from control B cells, however, by 686 less and 182 more abundant phospho-peptides (Figure S5D). Thus, B cells from AKT<sup>BOE</sup> mice respond to IgM engagement, but generate an altered response compared with controls.

B cells from AKT<sup>BOE</sup> mice have innate functions, a typical feature of *bona fide* MZ B cells, but have an impaired BCR functionality.

### Role of AKT in human splenic IgD<sup>+</sup>CD27<sup>hi</sup> B cell development

The finding that AKT plays a crucial role in mouse MZ B cell development and innate function led us to question the role of this signaling for human IgD<sup>+</sup>CD27<sup>+</sup> B cells proposed as equivalent to mouse MZ B cells,<sup>53</sup> although this notion is under debate.<sup>54,55</sup>

To address this question, we searched for genes providing an indication of AKT signaling in both mouse and human B cells. To this end, we compared the transcriptomes of human splenic IgD<sup>+</sup>CD27<sup>+</sup> (MZ-like) and IgD<sup>+</sup>CD27<sup>−</sup> (FO-like) B cells, and identified 1,496 differentially expressed genes ( $p < 0.05$ ) with a fold change superior to 1.5, corresponding to 2,298 Affymetrix probes (Tables S12 and S13). We next extracted from this list the genes for which we could find a mouse homolog based on the gene symbol, and we assessed the expression of these homologs in mouse MZ and FO B cells from AKT<sup>BOE</sup> and control

#### Figure 4. MZ-B cells from AKT<sup>BOE</sup> mice show normal innate functions

- (A) Flow cytometry plots showing TACI and CD138 expression on live B cells after stimulation with LPS for 48 h *in vitro*. Plasmacytes are gated as TACI<sup>+</sup>CD138<sup>+</sup> cells (left). Percentage of TACI<sup>+</sup>CD138<sup>+</sup> plasmacytes (right).
- (B) IgM concentration in supernatant of LPS-stimulated B cells from (A).
- (C) Splenic B cells from *Cd19-cre* and AKT<sup>BOE</sup> mice were stimulated *in vitro* for 24 h, and IL-6 (left) as well as IL-10 (right) were measured in supernatants. Pool of three experiments.
- (D) Isolated FO and MZ B cells from *Cd19-cre* and MZ B cells from AKT<sup>BOE</sup> mice were stimulated *in vitro* for 24 h, and IL-6 (left) as well as IL-10 (right) were measured in supernatants. Pool of two experiments.
- (E) Data show NP-reactive IgM antibodies in serum from *Cd19-cre* (black squares;  $n = 5$ ) and AKT<sup>BOE</sup> mice (red circles;  $n = 6$ ) post immunization (p.i.) with NP-LPS. Representative of two independent experiments.
- (F) Data show NP-reactive IgM and IgG3 antibodies in serum from *Cd19-cre* (black squares;  $n = 7$ ) and AKT<sup>BOE</sup> mice (red circles;  $n = 7$ ) after immunization with NP-Ficoll. Representative of two independent experiments.
- (G) NP-reactive IgM and IgG1 antibodies in serum from *Cd19-cre* ( $n = 7$ ) and AKT<sup>BOE</sup> mice ( $n = 7$ ) after immunization with NP-CGG. Representative of three independent experiments. Data are shown as mean  $\pm$  SEM. Significance was calculated using two-tailed unpaired Student's *t* test with \* $p < 0.05$ , \*\* $p < 0.01$ , \*\*\* $p < 0.001$ . See also Figure S4.

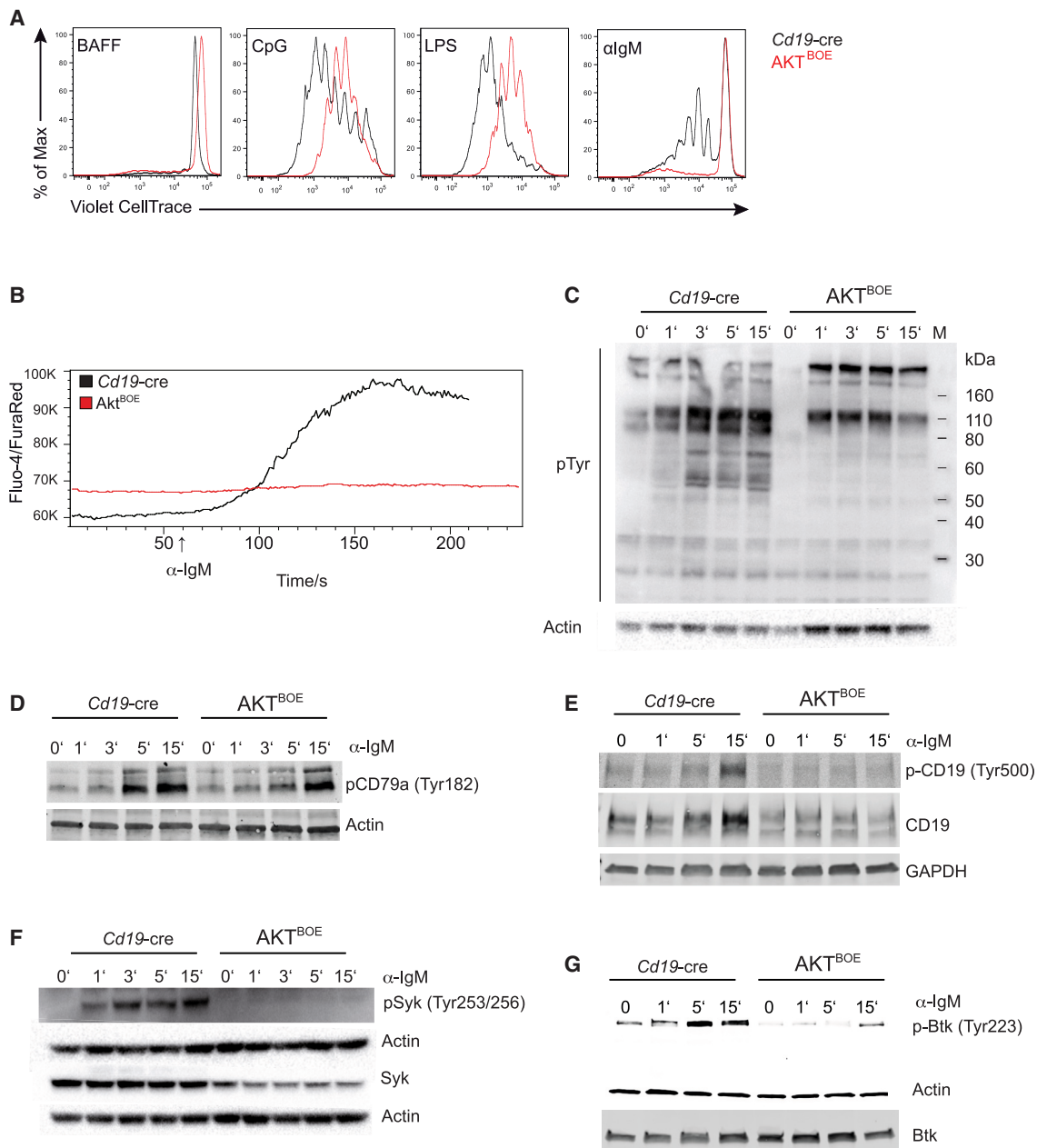


### Figure 5. Altered BCR signaling in AKT<sup>BOE</sup> B cells

(A) B cells from *Cd19-cre* and *AKT<sup>BOE</sup>* mice were labeled with CellTrace Violet, stimulated for 72 h, and analyzed by flow cytometry. Representative from three experiments with  $n \geq 3$  mice per genotype.

(B)  $Ca^{2+}$  flux in live  $CD19^+$  B cells from *AKT<sup>BOE</sup>* and *Cd19-cre* mice after stimulation with  $\alpha$ IgM (5  $\mu$ g/mL, indicated by arrow). Data representative of three independent experiments with two mice per genotype.

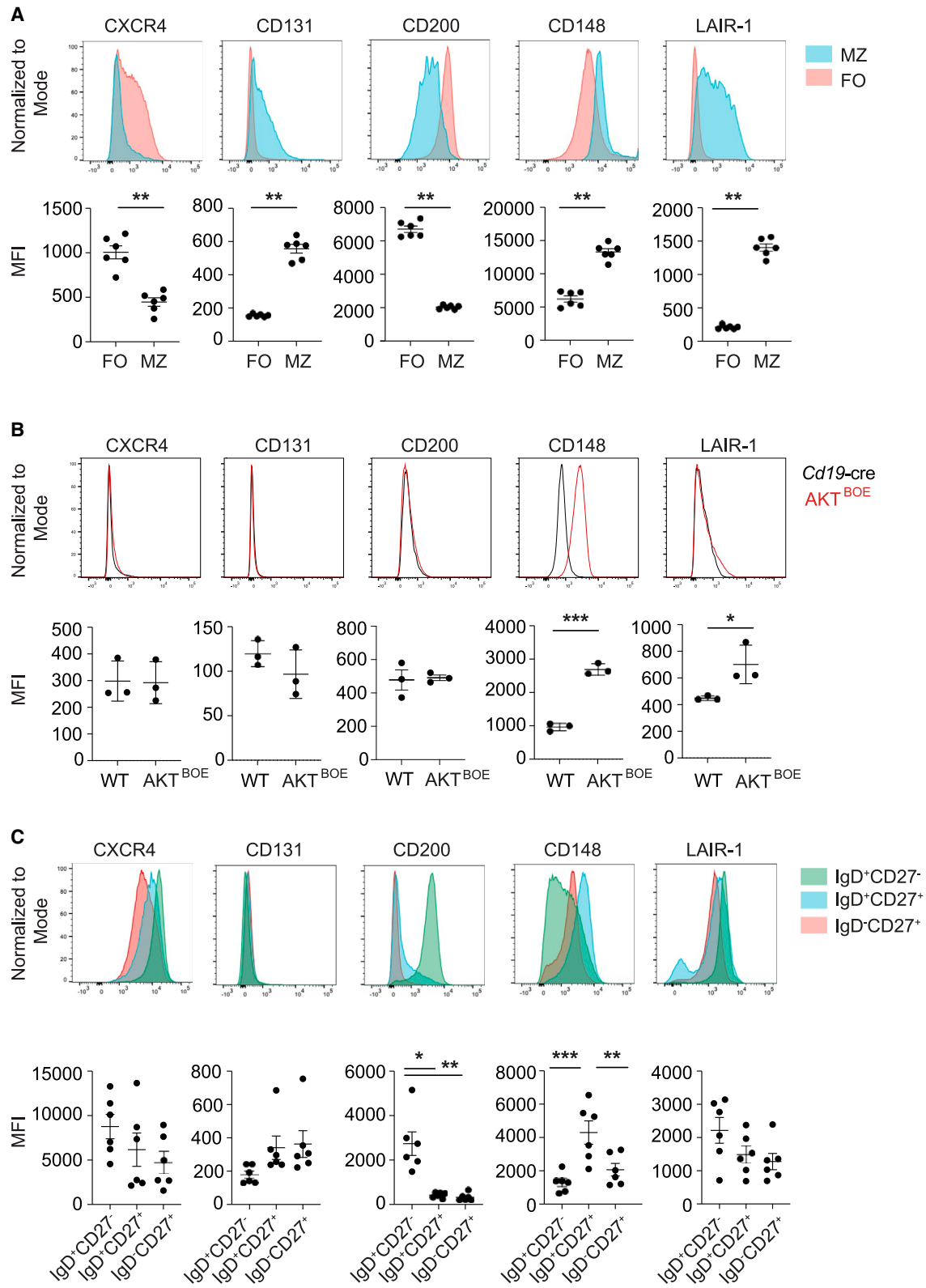
(C) Western blot showing phosphorylated tyrosine (pTyr) in B cells from *AKT<sup>BOE</sup>* and *Cd19-cre* mice after stimulation with  $\alpha$ IgM (5  $\mu$ g/mL). Data representative of three independent experiments.

(D) Western blot showing phosphorylated CD79 $\alpha$  in B cells from *AKT<sup>BOE</sup>* and *Cd19-cre* mice after stimulation with  $\alpha$ IgM (5  $\mu$ g/mL) for indicated time points. Actin was used as loading control. Data representative of three independent experiments.

(E) Western blot showing phosphorylated CD19 in B cells from *AKT<sup>BOE</sup>* and *Cd19-cre* mice after stimulation with  $\alpha$ IgM (5  $\mu$ g/mL). CD19 and GAPDH were used as loading controls. Data representative of three independent experiments.

(F) Western blot showing phosphorylated Syk and total Syk levels in B cells from *AKT<sup>BOE</sup>* and *Cd19-cre* mice after stimulation with  $\alpha$ IgM (5  $\mu$ g/mL) for indicated time points. Actin was used as loading control. Data representative of two independent experiments.

(G) Western blot showing phosphorylated and total Btk in B cells from *AKT<sup>BOE</sup>* and *Cd19-cre* mice after stimulation with  $\alpha$ IgM (5  $\mu$ g/mL) for indicated time points. Actin and Btk were used as loading controls. Data representative of three independent experiments. See also [Figure S5](#).



(legend on next page)

mice. This led us to identify 128 genes differentially expressed (1) between IgD<sup>+</sup>CD27<sup>+</sup> and IgD<sup>+</sup>CD27<sup>-</sup> B cells, (2) between mouse MZ B cells and FO B cells, and (3) that were controlled by AKT (i.e., differentially expressed between MZ-like B cells from AKT<sup>BOE</sup> mice and FO B cells from control mice) (Table S14). These contained 13 transcriptional regulators, including *Hes1*, *Satb1*, *Bcl6*, and *Hopx* (Figure S6A), and several transmembrane receptors, including *Lair1*, *Csf2rb*, *Cd9*, *Ccr1*, *Clic4*, *Sor11*, *Hvcn1*, *Cxcr4*, *Tmem64*, *Ccr7*, *Cd148* (*Ptprf*), and *Cd200* (Figure S6B).

To validate these results, we quantified the expression of these receptors on mouse and human splenic B cells by flow cytometry (Figure 6). Mouse MZ B cells displayed higher expression of CD131, CD148, and LAIR-1 than FO B cells, while their expression of CXCR4 and CD200 was lower (Figure 6A). To identify receptors whose expression was proportional to AKT activity, we next compared their expression on MZ B cells from AKT<sup>BOE</sup> mice and MZ B cells from controls. This highlighted CD148, a phosphatase implicated in antibody responses to polysaccharides<sup>56</sup> (Figure 6B). This finding suggests that CD148 might provide a proxy for the level of AKT activity in these cells. For comparison, we analyzed the expression of CD45, another tyrosine phosphatase.<sup>57</sup> CD45 was expressed at relatively similar levels on the surface of FO and MZ B cells of control and AKT<sup>BOE</sup> mice (Figure S7A).

We next examined the expression level of these receptors on human splenic B cells. CD148 was expressed at higher level on IgD<sup>+</sup>CD27<sup>+</sup> B cells compared with both IgD<sup>+</sup>CD27<sup>-</sup> naive B cells and IgD<sup>-</sup>CD27<sup>+</sup> memory B cells (Figure 6C), while the expression of CD45 was relatively similar between B cell subsets (Figure S7B). Further phenotypic characterizations confirmed that IgD<sup>+</sup>CD27<sup>+</sup> B cells expressed higher levels of CD1c, IgM, and CD21 than IgD<sup>-</sup>CD27<sup>+</sup> and IgD<sup>+</sup>CD27<sup>-</sup> B cells (Figure 7A). Splenic CD27<sup>+</sup> B cell subsets can be subdivided into subpopulations according to their Ig isotype and their level of CD21 expression.<sup>58</sup> CD148 was found at higher levels on IgD<sup>+</sup>CD27<sup>+</sup> B cells than on IgD<sup>-</sup>CD27<sup>+</sup> B cells regardless of their CD21 expression level (Figure 7B), as previously reported.<sup>58</sup> Since the higher expression of CD148 on IgD<sup>+</sup>CD27<sup>+</sup> B cells suggested that these cells experienced higher AKT signaling than IgD<sup>+</sup>CD27<sup>-</sup> naive B cells and IgD<sup>-</sup>CD27<sup>+</sup> memory B cells at steady state, we sought to examine the link between CD148 expression and AKT in human B cells. To this end, we used the mantle cell lymphoma (MCL) cell line Rec-1, which overexpresses CD148,<sup>59</sup> and displays constitutive AKT signaling.<sup>60</sup> The pharmacological inhibition of AKT in Rec-1 cells with MK-2206 reduced CD148 expression at their surface (Figure 7C), which correlated with the diminution of intracellular phospho-AKT (Figure 7C). In addition, we analyzed B cells from patients

with autoimmune lymphoproliferative syndrome (ALPS), which is caused by a mutation in the gene encoding for FAS, because naive B cells display higher mammalian target of rapamycin (mTOR) and AKT signaling in these patients compared with controls.<sup>61</sup> Remarkably, IgD<sup>+</sup>CD27<sup>-</sup> B cells from ALPS patients displayed a higher CD148 expression than naive B cells from controls (Figure 7D). The analysis of three patients before and after treatment with the mTOR inhibitor rapamycin suggested that this treatment might reduce CD148 expression on naive B cells, although the difference before/after treatment was not significant on this limited number of patients (Figure 7D). Supporting the notion that splenic IgD<sup>+</sup>CD27<sup>+</sup> B cells experience higher AKT signaling than other B cell subsets, the analysis of intracellular FoxO1 localization by imaging flow cytometry showed a higher cytoplasm/nucleus ratio in IgD<sup>+</sup>CD27<sup>+</sup> MZ B cells than in both IgD<sup>+</sup>CD27<sup>-</sup> naive and IgD<sup>-</sup>CD27<sup>+</sup> memory B cells (Figure S7C). To test the role of AKT in IgD<sup>+</sup>CD27<sup>+</sup> MZ B development, we then used an *in vitro* B cell differentiation system in which IgD<sup>+</sup>CD27<sup>+</sup> B cells develop from their splenic progenitor in a NOTCH2-instructed manner.<sup>15</sup> Thus, immature splenic IgD<sup>+</sup>CD27<sup>-</sup> MEM55<sup>+</sup> ABCB1<sup>+</sup> B cells were isolated and cultured on stromal cells expressing or not DLL1 for 3 days, and IgD<sup>+</sup>CD27<sup>-</sup> B cells as well as MZ-like IgD<sup>+</sup>CD27<sup>+</sup> B cells were then characterized.<sup>15</sup> A fraction of the immature cells are already committed to becoming IgD<sup>+</sup>CD27<sup>+</sup> B cells and do not require NOTCH2 engagement for this process, yet DLL1 augments the formation of IgD<sup>+</sup>CD27<sup>+</sup> B cells, which allows studying the mechanism implicated in this commitment step.<sup>15</sup> Remarkably, the inhibition of AKT signaling in these cultures reduced the induction of IgD<sup>+</sup>CD27<sup>+</sup> cells by DLL1 (Figure S7D), indicating that their NOTCH2-mediated development occurred in an AKT-dependent manner. Furthermore, the IgD<sup>+</sup>CD27<sup>+</sup> cells generated in this *in vitro* culture system displayed a higher CD148 expression compared with IgD<sup>+</sup>CD27<sup>-</sup> B cells from the same culture (Figure S7E), thus recapitulating the distinctive phenotypic feature observed with their human splenic counterparts (Figure 6C).

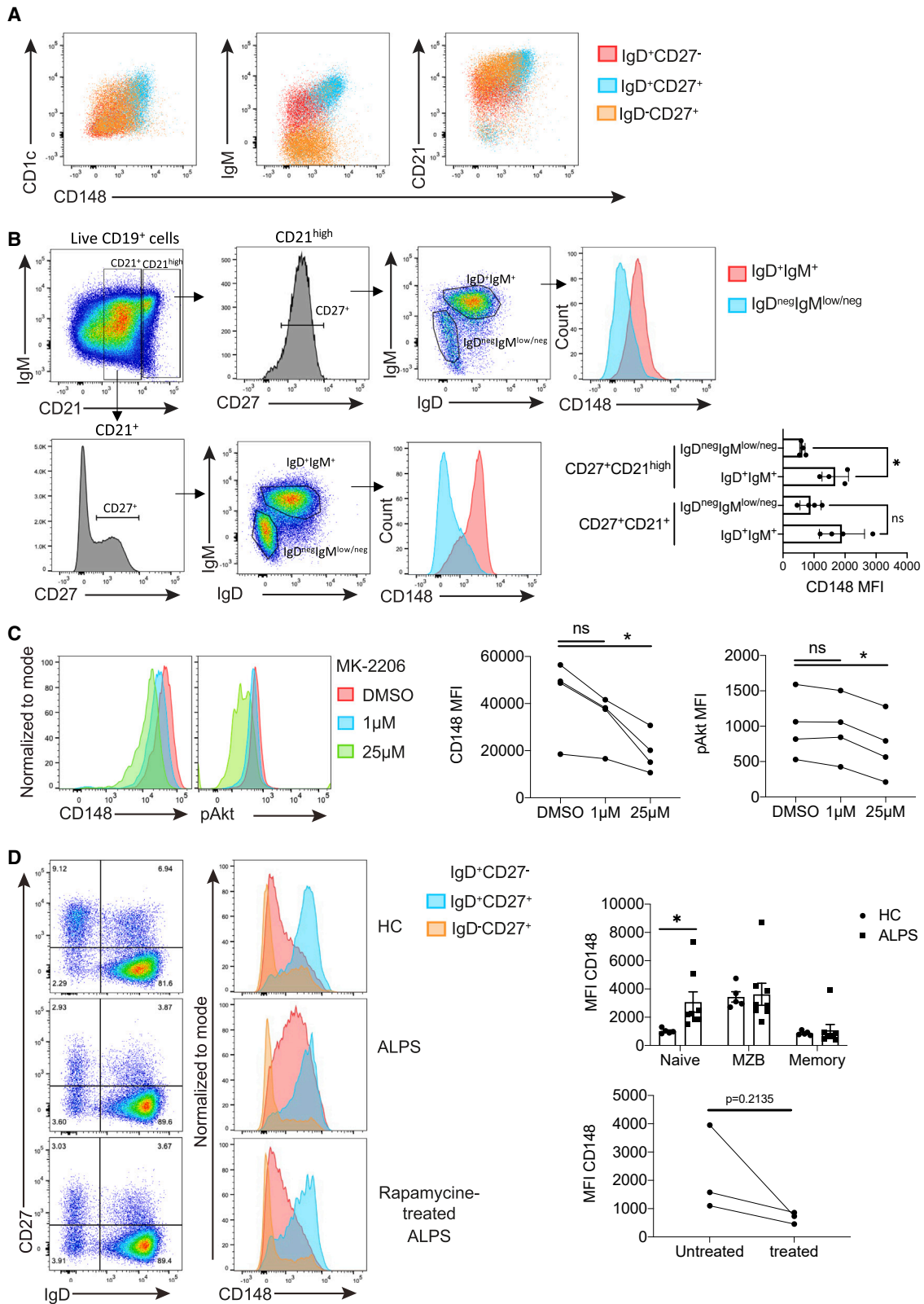
These data support the working hypothesis that human splenic IgD<sup>+</sup>CD27<sup>+</sup> B cells share with mouse MZ B cells an AKT-dependent development process, and they highlight that they share a high expression of CD148<sup>56</sup> as distinctive phenotypic features compared with other B cell subsets. These characteristics underline the similarity between these mouse and human B cell subsets.

## DISCUSSION

The signaling pathways controlling the development and function of MZ B cells remain incompletely defined. Here, we demonstrate that the genetic induction of AKT signaling in B cells is

### Figure 6. CD148 is upregulated on mouse and human MZ B cells

(A) Expression of indicated molecules on FO and MZ B cells from C57BL/6 mice. Flow cytometry plots representative of three independent experiments (top) and mean fluorescence intensity (MFI) values of indicated molecules (bottom) (n = 6 mice/group).  
(B) Expression of indicated molecules on MZ B cells from *Cd19-cre* and AKT<sup>BOE</sup> mice to identify markers controlled by AKT. Flow cytometry plots representative of two independent experiments (top) and MFI values of indicated molecules (bottom).  
(C) Expression of indicated molecules on human splenic IgD<sup>+</sup>CD27<sup>-</sup>, IgD<sup>+</sup>CD27<sup>+</sup> and IgD<sup>-</sup>CD27<sup>+</sup> B cells. Flow cytometry plots representative of six independent experiments (top) and MFI values of indicated molecules (bottom). Lines mark mean ± SEM. \*\*\*\*p < 0.0001, \*\*\*p < 0.001, \*\*p < 0.01, \*p < 0.05, using Mann-Whitney test (A), one-tailed unpaired Student's t test (B), and Kruskal-Wallis test (C). See also Figure S6.



(legend on next page)

sufficient to bias the B cell compartment toward an MZ-like phenotype having innate functions. We also show that increased AKT signaling is a key feature of human IgD<sup>+</sup>CD27<sup>+</sup> B cells, suggesting the conservation of this pathway in mice and humans.

The genetic increase of AKT activity selectively in B cells led to an almost complete conversion of the B cell compartment toward an MZ-like phenotype. Fetal liver chimera produced by reconstituting irradiated mice with fetal liver cells cultured *in vitro* and genetically deficient in both *Akt1* and *Akt2* indicated that AKT deficiency contributed to the accumulation of both FO and MZ B cells,<sup>26</sup> suggesting that increasing AKT signaling should raise the abundance of these two B cell subsets. In contrast to this prediction, the increased abundance of MZ-like B cells in AKT<sup>BOE</sup> mice was associated with an almost complete loss of FO B cells. The molecular profiling of these cells showed the modulation of genes known to influence the abundance of MZ B cells, such as *Ikaros* and *Hes1*, expressed at higher level in MZ B cells, as well as *Irf8*, *Klf2*, *Fli1*, *Bach2*, and *Bcl6* found at higher levels in FO B cells. Mice lacking *Ikaros* in B cells have fewer MZ B cells,<sup>36</sup> while mice deficient in *Irf8*, *Klf2*, and *Fli1* have more MZ B cells than controls.<sup>37–39</sup> The impact of AKT on these genes might thus directly contribute to the overabundance of MZ B cells in AKT<sup>BOE</sup> mice. Remarkably, B cells from AKT<sup>BOE</sup> mice also displayed an increased expression and activation of NOTCH2. A link between AKT activity and NOTCH activation was previously documented in other cell types,<sup>62,63</sup> and in B cell lymphoma.<sup>35</sup> In the latter case, the B cell-specific overexpression of AKT-C in a model of chronic lymphocytic leukemia (CLL) was associated with the activation of NOTCH signaling, which contributed to the progression of CLL toward Richter's transformation. Our data indicate that this link between AKT and NOTCH2 occurs in the absence of the TCL1 mutation required to drive CLL formation.<sup>35</sup> AKT<sup>BOE</sup> mice did not develop any lymphoma. Instead, their B cells showed a reduced proliferative activity, consistent with their reduced *Myc* expression.

The analysis of the transcriptome of MZ-like B cells failed to reveal any clear lineage- or pathway-specific signature. This likely reflects the establishment, in the context of a constitutive AKT signaling, of regulatory circuits having compensatory roles.

The accumulation of MZ-like B cells was associated with splenomegaly and an increased accumulation of all immune cell types analyzed, which were present in normal proportions. It is known that B cells control the maturation of secondary lymphoid organs<sup>64</sup> and their expansion under challenge<sup>65</sup> via processes involving the provision of lymphotoxin to stromal

cells.<sup>64,65</sup> The phenotype of AKT<sup>BOE</sup> mice suggests that MZ-like B cells promote the maturation and growth of the spleen.

The concept that AKT is a driver of MZ B cell formation is further corroborated by the analysis of mice overexpressing in B cells a *FoxO1* mutant that cannot be phosphorylated by AKT. These mice lacked MZ B cells, implying that FoxO1 blocks the expression of the genetic program leading to MZ B cell development. The inactivation of FoxO transcription factors by AKT is thus mandatory for MZ B cell development. The FOXO family comprises four members (FoxO1, FoxO3, FoxO4, and FoxO6) that bind to the same consensus sequence and can act in a redundant manner.<sup>66</sup> B cells express FoxO1, FoxO3a, and FoxO4.<sup>67</sup> It is possible that the deletion of *Foxo1* in B cells produced only a moderate increase in MZ B cells due to this redundancy.<sup>28</sup>

A distinctive functional feature of MZ B cells compared with FO B cells is their innate response to TLR agonists. B cells from AKT<sup>BOE</sup> mice displayed effective innate response both in terms of antibody and cytokine production. B cells from AKT<sup>BOE</sup> mice displayed a lower expression of *Bach2* and *Bcl6* than FO B cells, which might account for their effective differentiation into antibody-secreting cells (ASCs), because these transcription factors inhibit ASC differentiation. AKT signaling thus controls both the development and innate function of MZ B cells, providing a molecular link between these two aspects. These observations are consistent with recent data from Allman and colleagues, who showed that NOTCH2 and mTORC1 controlled the distinctive capacity of mouse MZ B cells to rapidly develop into plasmacytes in a cell-division-independent manner upon TLR stimulation, unlike FO B cells, which required cell proliferation.<sup>68</sup> Collectively, these data underline the importance of the AKT-mTORC1 pathway in the development and innate function of MZ B cells.

B cells from AKT<sup>BOE</sup> mice showed impaired BCR-mediated functions. This is reminiscent of observation in patients with mutations leading to hyperactivation of the PI3K-AKT pathway, who also displayed low levels of specific antibodies toward vaccine antigens of protein and polysaccharide types.<sup>69</sup> The effective function of TLR signaling while BCR signaling is impaired provides information on the interplay between TLR4 and BCR. Previous studies showed that the presence of the BCR was required for B cell proliferation and IL-10 production in response to LPS.<sup>70,71</sup> This relied on a genetic system removing the BCR from B cells. In our case, the BCR was present but part of its signaling was defective. The maintenance of TLR responsiveness suggests that distinct BCR-mediated activities are required

### Figure 7. CD148 and AKT signaling in human B cells

(A) Co-expression of CD148 with CD1c, IgM, and CD21 at the surface of human splenic B cell subsets.

(B) Gating strategy used to analyze the expression of CD148 in CD19<sup>+</sup>CD27<sup>+</sup>CD21<sup>high</sup> and CD19<sup>+</sup>CD27<sup>+</sup>CD21<sup>+</sup> splenic human B cells expressing different levels of IgM and IgD (left) and quantification of CD148 MFI in four samples (right). Statistical significance calculated using one-way ANOVA with Tukey correction; \*p < 0.05.

(C) Level of CD148 and phospho-AKT (pAkt) in live REC-1 cells treated with DMSO or MK-2206 for 24 h. Representative flow cytometry histogram (left) and MFI quantification (right). Four independent experiments; \*p < 0.05, using Kruskal-Wallis test.

(D) Flow cytometry plots showing CD27 and IgD on live blood CD19<sup>+</sup> B cells from healthy controls (HC; n = 5), ALPS patients (n = 8), and ALPS patients treated with rapamycin (n = 3) (left), as well as histograms showing CD148 expression on IgD<sup>+</sup>CD27<sup>-</sup>, IgD<sup>+</sup>CD27<sup>+</sup>, and IgD<sup>-</sup>CD27<sup>+</sup> B cells (middle panels) and their quantifications (right panels). Data represented as mean ± SEM; \*\*p < 0.01 using two-way ANOVA followed by Sidák's multiple comparisons test for top panel, and Wilcoxon test for bottom panel. See also Figure S7.

for innate and adaptive B cell responses, highlighting the possibility of their dissociation. Note that it might be possible that alteration in BCR signaling seen in B cells from AKT<sup>BOE</sup> mice might favor the development of MZ B cells.

The notion that IgD<sup>+</sup>CD27<sup>+</sup> B cells are equivalent to mouse MZ B cells predicts that their development follows conserved processes. In humans, available data suggest that they appear in spleen before IgD<sup>-</sup>CD27<sup>+</sup> B cells, being already detectable in 2- to 24-month-old infants and young children, with a frequency that then remains stable through life.<sup>58</sup> This suggests that the ontogeny of at least some of the IgD<sup>+</sup>CD27<sup>+</sup> B cells follows a distinct pathway compared with IgD<sup>-</sup>CD27<sup>+</sup> B cells. NOTCH2 is important for IgD<sup>+</sup>CD27<sup>+</sup> B cell development in human since the abundance of these cells is reduced in Alagille patients with a NOTCH2 haploinsufficiency.<sup>15</sup> IgD<sup>+</sup>CD27<sup>+</sup> B cells can be produced *in vitro* from human splenic progenitors in a NOTCH2-driven manner.<sup>15</sup> Remarkably, this NOTCH2-dependent development was dependent on AKT signaling. IgD<sup>+</sup>CD27<sup>+</sup> B cells also displayed a higher ratio of FoxO1 level in cytoplasm compared with nucleus and a higher expression of CD148, relative to other B cell subsets. Collectively, these data suggest that IgD<sup>+</sup>CD27<sup>+</sup> B cells undergo higher AKT signaling than other human B cell subsets, pointing to the conservation of this AKT role in mice and humans.

Our data highlight CD148 as a marker for MZ B cells conserved in mice and humans. CD148 is a phosphatase that regulates the activation of Src-family kinase, particularly Lyn.<sup>56</sup> It can bind to thrombospondin-1, which increases its catalytic activity,<sup>72</sup> and to heparan sulfate proteoglycan, a type 1 transmembrane proteoglycan expressed by fibroblasts and cells of the vasculature.<sup>73</sup> It might contribute to the functional property of MZ B cells because it facilitated antibody responses to polysaccharide TI-2 antigens in mice.<sup>56</sup> Our observations indicate that CD148 expression level is linked to the magnitude of AKT signaling in B cells. Following this reasoning, we analyzed CD148 expression on B cells from ALPS patients.<sup>61</sup> CD148 was expressed at a higher level on IgD<sup>+</sup>CD27<sup>-</sup> B cells from ALPS patients than controls. Noteworthy, these cells did not convert into IgD<sup>+</sup>CD27<sup>+</sup> B cells. Further investigations will be required to refine the notion that CD148 might be a surrogate to estimate the level PI3K-AKT-mTOR signaling in B cell subsets and to predict their functional properties, particularly their innate function and propensity to differentiate into ASC.

In conclusion, this study demonstrates that the AKT-FoxO axis is an on/off gate for MZ B cell development, controlling the expression of transcription factors and the activity of NOTCH2 that regulate this B cell ontogeny. AKT signaling additionally endows B cells with innate functions, a distinctive asset of MZ B cells compared with FO B cells. It contributes to the control of CD148 expression. In sum, AKT is a key orchestrator of MZ B cell development with conserved roles in mice and humans.

### Limitations of the study

A limitation of the study lies in the utilization of a genetic model with constitutive active expression of AKT in B cells. This model is unlikely to recapitulate the variations in AKT signaling that accompany B cell development and activation upon antigenic stimulation. Accordingly, MZ-like B cells from AKT<sup>BOE</sup> mice

display all key features of MZ B cells (phenotype, localization in spleen, and innate functions) and a closely related transcriptome, yet they also show some differences, including at the level of their transcriptome and the function of their BCR. Of note, patients with mutations leading to hyperactive PI3K-AKT pathway seem to be affected by a similar problem because they have low levels of specific antibodies toward vaccines.<sup>69</sup> These data suggest that the dynamic regulation of AKT signaling is central for proper BCR function, which will require further studies for a detailed molecular understanding.

### STAR★METHODS

Detailed methods are provided in the online version of this paper and include the following:

- KEY RESOURCES TABLE
- RESOURCE AVAILABILITY
  - Lead contact
  - Materials availability
  - Data and code availability
- EXPERIMENTAL MODEL AND SUBJECT DETAILS
  - Mice
  - Human samples
- METHOD DETAILS
  - Cell sorting of MZP and *in vitro* differentiation assay
  - Mouse cell purification and *in vitro* assays
  - Flow cytometry
  - Immunization and ELISA
  - Western blot analysis
  - Immunohistochemistry
  - Measurement of intracellular calcium flux
  - Microarray and statistical analysis
  - Gene array hybridization
- QUANTIFICATION AND STATISTICAL ANALYSIS

### SUPPLEMENTAL INFORMATION

Supplemental information can be found online at <https://doi.org/10.1016/j.celrep.2023.112378>.

### ACKNOWLEDGMENTS

We thank J. Kirsch, H. Schliemann, the Regine von Ramin Laboratory (DRFZ), Petra Adams-Quack and Elena Zurkowski (IMM, Mainz), and Michael Dussiot (IMAGINE) for excellent technical help. We thank E. Six and I. André (IMAGINE) for the OP9 and OP9-DLL1 cell lines. We thank V. Asnafi and E. Macintyre (INEM) for REC-1 cells. The N.H. lab was supported by the Fritz Thyssen Foundation, AZ 10.13.2.173 and by the DFG grant HO4440/1-1, HO4440/1-2, project number 318346496, SFB1292/2 TP20, and the Research Center Immunology (FZI). The S.F. lab is supported by ERC PREG-LAB 647696, AXA Chair Translational Immunology, Agence Nationale de la Recherche (ANR-16-CE18-0007-01), Chair of Excellence (Université Sorbonne Paris Cité). M.R. is supported by the DFG (SFB1160, B02). F.R.L. was funded by the Institut National de la Santé et de la Recherche Médicale (Inserm), the French government (managed by French National Research Agency [Agence Nationale de la Recherche] through the Investissements d'avenir program [Institut Hospitalo-Universitaire Imagine, grant reference, ANR-10-IAHU-01]; Recherche Hospitalo-Universitaire, grant reference, ANR-18-RHUS-0010]), and other grants from the Agence National de la Recherche (ANR-18-CE17-0001).

Action), the Fondation pour la Recherche Médicale (grant reference, Equipe FRM EQU202103012670).

#### AUTHOR CONTRIBUTIONS

E.M.C., M.E.B., S.R., J.F.V., V.K., T.M., B.M., M.A.M., F.W., B.T., C.P., H.L., N.Y., R.M., M.D., S.W., L.J., S.T., U.D., A.R.E., C.K., J.S., A.M., and F.T.W. performed experiments and provided reagents. P.B., J.C.W., C.A.R., F.R.L., and M.R. designed experiments and supervised data analysis. N.H. and S.F. designed the project, analyzed data, and wrote the manuscript.

#### DECLARATION OF INTERESTS

The authors declare no competing interests.

Received: January 28, 2021

Revised: December 14, 2022

Accepted: March 27, 2023

Published: April 14, 2023

#### REFERENCES

- Grasseau, A., Boudigou, M., Le Pottier, L., Chriti, N., Cornec, D., Pers, J.O., Renaudineau, Y., and Hillion, S. (2020). Innate B cells: the archetype of protective immune cells. *Clin. Rev. Allergy Immunol.* *58*, 92–106. <https://doi.org/10.1007/s12016-019-08748-7>.
- Cerutti, A., Cols, M., and Puga, I. (2013). Marginal zone B cells: virtues of innate-like antibody-producing lymphocytes. *Nat. Rev. Immunol.* *13*, 118–132. <https://doi.org/10.1038/nri3383>.
- Shen, P., Roch, T., Lampropoulou, V., O'Connor, R.A., Stervbo, U., Hilgenberg, E., Ries, S., Dang, V.D., Jaimes, Y., Daridon, C., et al. (2014). IL-35-producing B cells are critical regulators of immunity during autoimmune and infectious diseases. *Nature* *507*, 366–370. <https://doi.org/10.1038/nature12979>.
- Allman, D., and Pillai, S. (2008). Peripheral B cell subsets. *Curr. Opin. Immunol.* *20*, 149–157. <https://doi.org/10.1016/j.coi.2008.03.014>.
- Tull, T.J., Pitcher, M.J., Guesdon, W., Siu, J.H.Y., Lebrero-Fernández, C., Zhao, Y., Petrov, N., Heck, S., Ellis, R., Dhami, P., et al. (2021). Human marginal zone B cell development from early T2 progenitors. *J. Exp. Med.* *218*, e20202001. <https://doi.org/10.1084/jem.20202001>.
- Wang, H., Morse, H.C., 3rd, and Bolland, S. (2020). Transcriptional control of mature B cell fates. *Trends Immunol.* *41*, 601–613. <https://doi.org/10.1016/j.it.2020.04.011>.
- Pillai, S., and Cariappa, A. (2009). The follicular versus marginal zone B lymphocyte cell fate decision. *Nat. Rev. Immunol.* *9*, 767–777. <https://doi.org/10.1038/nri2656>.
- Saito, T., Chiba, S., Ichikawa, M., Kunisato, A., Asai, T., Shimizu, K., Yamaguchi, T., Yamamoto, G., Seo, S., Kumano, K., et al. (2003). Notch2 is preferentially expressed in mature B cells and indispensable for marginal zone B lineage development. *Immunity* *18*, 675–685. [https://doi.org/10.1016/s1074-7613\(03\)00111-0](https://doi.org/10.1016/s1074-7613(03)00111-0).
- Hampel, F., Ehrenberg, S., Hojer, C., Draeseke, A., Marschall-Schröter, G., Kühn, R., Mack, B., Gires, O., Vahl, C.J., Schmidt-Suppran, M., et al. (2011). CD19-independent instruction of murine marginal zone B-cell development by constitutive Notch2 signaling. *Blood* *118*, 6321–6331. <https://doi.org/10.1182/blood-2010-12-325944>.
- Yu, J., Zanotti, S., Walia, B., Jellison, E., Sanjay, A., and Canalis, E. (2018). The Hajdu Cheney mutation is a determinant of B-cell allocation of the splenic marginal zone. *Am. J. Pathol.* *188*, 149–159. <https://doi.org/10.1016/j.ajpath.2017.09.010>.
- Lechner, M., Engleitner, T., Babushku, T., Schmidt-Suppran, M., Rad, R., Strobl, L.J., and Zimmer-Strobl, U. (2021). Notch2-mediated plasticity between marginal zone and follicular B cells. *Nat. Commun.* *12*, 1111. <https://doi.org/10.1038/s41467-021-21359-1>.
- Hozumi, K., Negishi, N., Suzuki, D., Abe, N., Sotomaru, Y., Tamaoki, N., Mailhos, C., Ish-Horowicz, D., Habu, S., and Owen, M.J. (2004). Delta-like 1 is necessary for the generation of marginal zone B cells but not T cells in vivo. *Nat. Immunol.* *5*, 638–644. <https://doi.org/10.1038/ni1075>.
- Tan, J.B., Xu, K., Cretegnny, K., Visan, I., Yuan, J.S., Egan, S.E., and Guidos, C.J. (2009). Lunatic and manic fringe cooperatively enhance marginal zone B cell precursor competition for delta-like 1 in splenic endothelial niches. *Immunity* *30*, 254–263. <https://doi.org/10.1016/j.immuni.2008.12.016>.
- Fasnacht, N., Huang, H.Y., Koch, U., Favre, S., Auderset, F., Chai, Q., Onder, L., Kallert, S., Pinschewer, D.D., MacDonald, H.R., et al. (2014). Specific fibroblastic niches in secondary lymphoid organs orchestrate distinct Notch-regulated immune responses. *J. Exp. Med.* *211*, 2265–2279. <https://doi.org/10.1084/jem.20132528>.
- Descatoire, M., Weller, S., Irtan, S., Sarnacki, S., Feuillard, J., Storck, S., Guiochon-Mantel, A., Bouligand, J., Morali, A., Cohen, J., et al. (2014). Identification of a human splenic marginal zone B cell precursor with NOTCH2-dependent differentiation properties. *J. Exp. Med.* *211*, 987–1000. <https://doi.org/10.1084/jem.20132203>.
- Tanigaki, K., Han, H., Yamamoto, N., Tashiro, K., Ikegawa, M., Kuroda, K., Suzuki, A., Nakano, T., and Honjo, T. (2002). Notch-RBP-J signaling is involved in cell fate determination of marginal zone B cells. *Nat. Immunol.* *3*, 443–450. <https://doi.org/10.1038/ni793>.
- Ayaz, F., and Osborne, B.A. (2014). Non-canonical notch signaling in cancer and immunity. *Front. Oncol.* *4*, 345. <https://doi.org/10.3389/fonc.2014.00345>.
- Wen, L., Brill-Dashoff, J., Shinton, S.A., Asano, M., Hardy, R.R., and Hayakawa, K. (2005). Evidence of marginal-zone B cell-positive selection in spleen. *Immunity* *23*, 297–308. <https://doi.org/10.1016/j.immuni.2005.08.007>.
- Noviski, M., Tan, C., Huizar, J., Vykunta, V., Mueller, J.L., and Zikherman, J. (2019). Optimal development of mature B cells requires recognition of endogenous antigens. *J. Immunol.* *203*, 418–428. <https://doi.org/10.4049/jimmunol.1900175>.
- Niir, H., and Clark, E.A. (2003). Branches of the B cell antigen receptor pathway are directed by protein conduits Bam32 and Carma1. *Immunity* *19*, 637–640. [https://doi.org/10.1016/s1074-7613\(03\)00303-0](https://doi.org/10.1016/s1074-7613(03)00303-0).
- Engel, P., Zhou, L.J., Ord, D.C., Sato, S., Koller, B., and Tedder, T.F. (1995). Abnormal B lymphocyte development, activation, and differentiation in mice that lack or overexpress the CD19 signal transduction molecule. *Immunity* *3*, 39–50. [https://doi.org/10.1016/1074-7613\(95\)90157-4](https://doi.org/10.1016/1074-7613(95)90157-4).
- Rickert, R.C., Rajewsky, K., and Roes, J. (1995). Impairment of T-cell-dependent B-cell responses and B-1 cell development in CD19-deficient mice. *Nature* *376*, 352–355. <https://doi.org/10.1038/376352a0>.
- Sato, S., Steeber, D.A., and Tedder, T.F. (1995). The CD19 signal transduction molecule is a response regulator of B-lymphocyte differentiation. *Proc. Natl. Acad. Sci. USA* *92*, 11558–11562. <https://doi.org/10.1073/pnas.92.25.11558>.
- Janas, M.L., Hodson, D., Stamatakis, Z., Hill, S., Welch, K., Gambardella, L., Trotman, L.C., Pandolfi, P.P., Vigorito, E., and Turner, M. (2008). The effect of deleting p110delta on the phenotype and function of PTEN-deficient B cells. *J. Immunol.* *180*, 739–746. <https://doi.org/10.4049/jimmunol.180.2.739>.
- Martin, F., and Kearney, J.F. (2000). B-cell subsets and the mature preimmune repertoire. Marginal zone and B1 B cells as part of a "natural immune memory". *Immunol. Rev.* *175*, 70–79.
- Calamito, M., Juntilla, M.M., Thomas, M., Northrup, D.L., Rathmell, J., Birnbaum, M.J., Koretzky, G., and Allman, D. (2010). Akt1 and Akt2 promote peripheral B-cell maturation and survival. *Blood* *115*, 4043–4050. <https://doi.org/10.1182/blood-2009-09-241638>.
- Anzelon, A.N., Wu, H., and Rickert, R.C. (2003). Pten inactivation alters peripheral B lymphocyte fate and reconstitutes CD19 function. *Nat. Immunol.* *4*, 287–294. <https://doi.org/10.1038/ni892>.

28. Chen, J., Limon, J.J., Blanc, C., Peng, S.L., and Fruman, D.A. (2010). Foxo1 regulates marginal zone B-cell development. *Eur. J. Immunol.* *40*, 1890–1896. <https://doi.org/10.1002/eji.200939817>.
29. Matsuzaki, H., Daitoku, H., Hatta, M., Tanaka, K., and Fukamizu, A. (2003). Insulin-induced phosphorylation of FKHR (Foxo1) targets to proteasomal degradation. *Proc. Natl. Acad. Sci. USA* *100*, 11285–11290. <https://doi.org/10.1073/pnas.1934283100>.
30. Song, M.S., Salmena, L., and Pandolfi, P.P. (2012). The functions and regulation of the PTEN tumour suppressor. *Nat. Rev. Mol. Cell Biol.* *13*, 283–296. <https://doi.org/10.1038/nrm3330>.
31. Blanco-Aparicio, C., Renner, O., Leal, J.F.M., and Carnero, A. (2007). PTEN, more than the AKT pathway. *Carcinogenesis* *28*, 1379–1386. <https://doi.org/10.1093/carcin/bgm052>.
32. Lee, Y.R., Chen, M., and Pandolfi, P.P. (2018). The functions and regulation of the PTEN tumour suppressor: new modes and prospects. *Nat. Rev. Mol. Cell Biol.* *19*, 547–562. <https://doi.org/10.1038/s41580-018-0015-0>.
33. Yudushkin, I. (2020). Control of Akt activity and substrate phosphorylation in cells. *IUBMB Life* *72*, 1115–1125. <https://doi.org/10.1002/iub.2264>.
34. Otipoby, K.L., Sasaki, Y., Schmidt-Suppran, M., Patke, A., Gareus, R., Pasparakis, M., Tarakhovskiy, A., and Rajewsky, K. (2008). BAFF activates Akt and Erk through BAFF-R in an IKK1-dependent manner in primary mouse B cells. *Proc. Natl. Acad. Sci. USA* *105*, 12435–12438. <https://doi.org/10.1073/pnas.0805460105>.
35. Kohlhaas, V., Blakemore, S.J., Al-Maarri, M., Nickel, N., Pal, M., Roth, A., Hoevelmeyer, N., Schafer, S.C., Knittel, G., Lohneis, P., et al. (2020). Active AKT signaling triggers CLL towards Richter's transformation via over-activation of Notch1. *Blood* *137*, 646–660. <https://doi.org/10.1182/blood.2020005734>.
36. Schwickert, T.A., Tagoh, H., Schindler, K., Fischer, M., Jaritz, M., and Buslinger, M. (2019). Ikaros prevents autoimmunity by controlling energy and Toll-like receptor signaling in B cells. *Nat. Immunol.* *20*, 1517–1529. <https://doi.org/10.1038/s41590-019-0490-2>.
37. Feng, J., Wang, H., Shin, D.M., Masiuk, M., Qi, C.F., and Morse, H.C., 3rd. (2011). IFN regulatory factor 8 restricts the size of the marginal zone and follicular B cell pools. *J. Immunol.* *186*, 1458–1466. <https://doi.org/10.4049/jimmunol.1001950>.
38. Alles, M., Turchinovich, G., Zhang, P., Schuh, W., Agenès, F., and Kirberg, J. (2014). Leukocyte beta7 integrin targeted by Kruppel-like factors. *J. Immunol.* *193*, 1737–1746. <https://doi.org/10.4049/jimmunol.1302613>.
39. Zhang, X.K., Moussa, O., LaRue, A., Bradshaw, S., Molano, I., Spyropoulos, D.D., Gilkeson, G.S., and Watson, D.K. (2008). The transcription factor Fli-1 modulates marginal zone and follicular B cell development in mice. *J. Immunol.* *181*, 1644–1654. <https://doi.org/10.4049/jimmunol.181.3.1644>.
40. Hammad, H., Vanderkerken, M., Pouliot, P., Deswarte, K., Toussaint, W., Vergote, K., Vandersarren, L., Janssens, S., Ramou, I., Savvides, S.N., et al. (2017). Transitional B cells commit to marginal zone B cell fate by Taok3-mediated surface expression of ADAM10. *Nat. Immunol.* *18*, 313–320. <https://doi.org/10.1038/ni.3657>.
41. Lownik, J.C., Wimberly, J.L., Takahashi-Ruiz, L., and Martin, R.K. (2020). B cell ADAM17 controls T cell independent humoral immune responses through regulation of TACI and CD138. *Biochem. Biophys. Res. Commun.* *522*, 442–447. <https://doi.org/10.1016/j.bbrc.2019.11.124>.
42. Fernández, D., Ortiz, M., Rodríguez, L., García, A., Martínez, D., and Moreno de Alborán, I. (2013). The proto-oncogene c-myc regulates antibody secretion and Ig class switch recombination. *J. Immunol.* *190*, 6135–6144. <https://doi.org/10.4049/jimmunol.1300712>.
43. Calado, D.P., Sasaki, Y., Godinho, S.A., Pellerin, A., Köchert, K., Sleckman, B.P., de Alborán, I.M., Janz, M., Rodig, S., and Rajewsky, K. (2012). The cell-cycle regulator c-Myc is essential for the formation and maintenance of germinal centers. *Nat. Immunol.* *13*, 1092–1100. <https://doi.org/10.1038/ni.2418>.
44. Meyer-Bahlburg, A., Bandaranayake, A.D., Andrews, S.F., and Rawlings, D.J. (2009). Reduced c-myc expression levels limit follicular mature B cell cycling in response to TLR signals. *J. Immunol.* *182*, 4065–4075. <https://doi.org/10.4049/jimmunol.0802961>.
45. Vaidyanathan, B., Chaudhry, A., Yewdell, W.T., Angeletti, D., Yen, W.F., Wheatley, A.K., Bradfield, C.A., McDermott, A.B., Yewdell, J.W., Rudensky, A.Y., and Chaudhuri, J. (2017). The aryl hydrocarbon receptor controls cell-fate decisions in B cells. *J. Exp. Med.* *214*, 197–208. <https://doi.org/10.1084/jem.20160789>.
46. Buhl, A.M., Pleiman, C.M., Rickert, R.C., and Cambier, J.C. (1997). Qualitative regulation of B cell antigen receptor signaling by CD19: selective requirement for PI3-kinase activation, inositol-1,4,5-trisphosphate production and Ca<sup>2+</sup> mobilization. *J. Exp. Med.* *186*, 1897–1910. <https://doi.org/10.1084/jem.186.11.1897>.
47. Vanhaesebroeck, B., Guillermet-Guibert, J., Graupera, M., and Bilanges, B. (2010). The emerging mechanisms of isoform-specific PI3K signalling. *Nat. Rev. Mol. Cell Biol.* *11*, 329–341. <https://doi.org/10.1038/nrm2882>.
48. Lien, E.C., Dibble, C.C., and Toker, A. (2017). PI3K signaling in cancer: beyond AKT. *Curr. Opin. Cell Biol.* *45*, 62–71. <https://doi.org/10.1016/j.ceb.2017.02.007>.
49. Stöhr, O., Schilbach, K., Moll, L., Hettich, M.M., Freude, S., Wunderlich, F.T., Ernst, M., Zemva, J., Brüning, J.C., Krone, W., et al. (2013). Insulin receptor signaling mediates APP processing and beta-amyloid accumulation without altering survival in a transgenic mouse model of Alzheimer's disease. *Age (Dordr)* *35*, 83–101. <https://doi.org/10.1007/s11357-011-9333-2>.
50. Catrina, I.E., Bayer, L.V., Yanez, G., McLaughlin, J.M., Malaczek, K., Bagaeva, E., Marras, S.A.E., and Bratu, D.P. (2016). The temporally controlled expression of Drongo, the fruit fly homolog of AGFG1, is achieved in female germline cells via P-bodies and its localization requires functional Rab11. *RNA Biol.* *13*, 1117–1132. <https://doi.org/10.1080/15476286.2016.1218592>.
51. Tcherkezian, J., Cargnello, M., Romeo, Y., Huttlin, E.L., Lavoie, G., Gygi, S.P., and Roux, P.P. (2014). Proteomic analysis of cap-dependent translation identifies LARP1 as a key regulator of 5'TOP mRNA translation. *Genes Dev.* *28*, 357–371. <https://doi.org/10.1101/gad.231407.113>.
52. Kai, M. (2016). Roles of RNA-binding proteins in DNA damage response. *Int. J. Mol. Sci.* *17*, 310. <https://doi.org/10.3390/ijms17030310>.
53. Weill, J.C., Weller, S., and Reynaud, C.A. (2009). Human marginal zone B cells. *Annu. Rev. Immunol.* *27*, 267–285. <https://doi.org/10.1146/annurev.immunol.021908.132607>.
54. Budeus, B., Schweigle de Reynoso, S., Przekopowicz, M., Hoffmann, D., Seifert, M., and Küppers, R. (2015). Complexity of the human memory B-cell compartment is determined by the versatility of clonal diversification in germinal centers. *Proc. Natl. Acad. Sci. USA* *112*, E5281–E5289. <https://doi.org/10.1073/pnas.1511270112>.
55. Bagnara, D., Squillario, M., Kipling, D., Mora, T., Walczak, A.M., Da Silva, L., Weller, S., Dunn-Walters, D.K., Weill, J.C., and Reynaud, C.A. (2015). A reassessment of IgM memory subsets in humans. *J. Immunol.* *195*, 3716–3724. <https://doi.org/10.4049/jimmunol.1500753>.
56. Skrzypczynska, K.M., Zhu, J.W., and Weiss, A. (2016). Positive regulation of Lyn kinase by CD148 is required for B cell receptor signaling in B1 but not B2 B cells. *Immunity* *45*, 1232–1244. <https://doi.org/10.1016/j.immuni.2016.10.013>.
57. Zhu, J.W., Brdicka, T., Katsumoto, T.R., Lin, J., and Weiss, A. (2008). Structurally distinct phosphatases CD45 and CD148 both regulate B cell and macrophage immunoreceptor signaling. *Immunity* *28*, 183–196. <https://doi.org/10.1016/j.immuni.2007.11.024>.
58. Kibler, A., Budeus, B., Homp, E., Bronischewski, K., Berg, V., Sellmann, L., Murke, F., Heinold, A., Heinemann, F.M., Lindemann, M., et al. (2021). Systematic memory B cell archiving and random display shape the human splenic marginal zone throughout life. *J. Exp. Med.* *218*, e20201952. <https://doi.org/10.1084/jem.20201952>.

59. Miguet, L., Béchade, G., Fornecker, L., Zink, E., Felden, C., Gervais, C., Herbrecht, R., Van Dorsseleer, A., Mauvieux, L., and Sanglier-Cianferani, S. (2009). Proteomic analysis of malignant B-cell derived microparticles reveals CD148 as a potentially useful antigenic biomarker for mantle cell lymphoma diagnosis. *J. Proteome Res.* 8, 3346–3354. <https://doi.org/10.1021/pr801102c>.
60. Psyrrri, A., Papageorgiou, S., Liakata, E., Scorilas, A., Rontogianni, D., Kontos, C.K., Argyriou, P., Pectasides, D., Harhalakis, N., Pappa, V., et al. (2009). Phosphatidylinositol 3'-kinase catalytic subunit alpha gene amplification contributes to the pathogenesis of mantle cell lymphoma. *Clin. Cancer Res.* 15, 5724–5732. <https://doi.org/10.1158/1078-0432.CCR-08-3215>.
61. Staniek, J., Kalina, T., Andrieux, G., Boerris, M., Janowska, I., Fuentes, M., Diez, P., Bakardjieva, M., Stancikova, J., Raabe, J., et al. Non-apoptotic FAS Signaling Controls CD40-dependent mTOR Activation and Balances Extrafollicular versus Germinal Center Fate in Human B Cells. submitted. *Science Immunology*.
62. Varga, J., Nicolas, A., Petrocelli, V., Pesic, M., Mahmoud, A., Michels, B.E., Eftlioglu, E., Yepes, D., Häupl, B., Ziegler, P.K., et al. (2020). AKT-dependent NOTCH3 activation drives tumor progression in a model of mesenchymal colorectal cancer. *J. Exp. Med.* 217, e20191515. <https://doi.org/10.1084/jem.20191515>.
63. Calzavara, E., Chiamonte, R., Cesana, D., Basile, A., Sherbet, G.V., and Comi, P. (2008). Reciprocal regulation of Notch and PI3K/Akt signalling in T-ALL cells in vitro. *J. Cell. Biochem.* 103, 1405–1412. <https://doi.org/10.1002/jcb.21527>.
64. Ngo, V.N., Cornall, R.J., and Cyster, J.G. (2001). Splenic T zone development is B cell dependent. *J. Exp. Med.* 194, 1649–1660. <https://doi.org/10.1084/jem.194.11.1649>.
65. Kumar, V., Scandella, E., Danuser, R., Onder, L., Nitschké, M., Fukui, Y., Halin, C., Ludewig, B., and Stein, J.V. (2010). Global lymphoid tissue remodeling during a viral infection is orchestrated by a B cell-lymphotoxin-dependent pathway. *Blood* 115, 4725–4733. <https://doi.org/10.1182/blood-2009-10-250118>.
66. Eijkelenboom, A., and Burgering, B.M.T. (2013). FOXOs: signalling integrators for homeostasis maintenance. *Nat. Rev. Mol. Cell Biol.* 14, 83–97. <https://doi.org/10.1038/nrm3507>.
67. Hinman, R.M., Bushanam, J.N., Nichols, W.A., and Satterthwaite, A.B. (2007). B cell receptor signaling down-regulates forkhead box transcription factor class O 1 mRNA expression via phosphatidylinositol 3-kinase and Bruton's tyrosine kinase. *J. Immunol.* 178, 740–747. <https://doi.org/10.4049/jimmunol.178.2.740>.
68. Gaudette, B.T., Roman, C.J., Ochoa, T.A., Gómez Atria, D., Jones, D.D., Siebel, C.W., Maillard, I., and Allman, D. (2021). Resting innate-like B cells leverage sustained Notch2/mTORC1 signaling to achieve rapid and mitosis-independent plasma cell differentiation. *J. Clin. Invest.* 131, e151975. <https://doi.org/10.1172/JCI151975>.
69. Angulo, I., Vadas, O., Garçon, F., Banham-Hall, E., Plagnol, V., Leahy, T.R., Baxendale, H., Coulter, T., Curtis, J., Wu, C., et al. (2013). Phosphoinositide 3-kinase delta gene mutation predisposes to respiratory infection and airway damage. *Science* 342, 866–871. <https://doi.org/10.1126/science.1243292>.
70. Schweighoffer, E., Nys, J., Vanes, L., Smithers, N., and Tybulewicz, V.L.J. (2017). TLR4 signals in B lymphocytes are transduced via the B cell antigen receptor and SYK. *J. Exp. Med.* 214, 1269–1280. <https://doi.org/10.1084/jem.20161117>.
71. Otipoby, K.L., Waisman, A., Derudder, E., Srinivasan, L., Franklin, A., and Rajewsky, K. (2015). The B-cell antigen receptor integrates adaptive and innate immune signals. *Proc. Natl. Acad. Sci. USA* 112, 12145–12150. <https://doi.org/10.1073/pnas.1516428112>.
72. Takahashi, K., Mernaugh, R.L., Friedman, D.B., Weller, R., Tsuboi, N., Yamashita, H., Quaranta, V., and Takahashi, T. (2012). Thrombospondin-1 acts as a ligand for CD148 tyrosine phosphatase. *Proc. Natl. Acad. Sci. USA* 109, 1985–1990. <https://doi.org/10.1073/pnas.1106171109>.
73. Whiteford, J.R., Xian, X., Chaussade, C., Vanhaesebroeck, B., Nourshargh, S., and Couchman, J.R. (2011). Syndecan-2 is a novel ligand for the protein tyrosine phosphatase receptor CD148. *Mol. Biol. Cell* 22, 3609–3624. <https://doi.org/10.1091/mbc.E11-02-0099>.
74. Six, E.M., Benjelloun, F., Garrigue, A., Bonhomme, D., Morillon, E., Rouiller, J., Cacavelli, L., Blondeau, J., Beldjord, K., Hacein-Bey-Abina, S., et al. (2011). Cytokines and culture medium have a major impact on human in vitro T-cell differentiation. *Blood Cells Mol. Dis.* 47, 72–78. <https://doi.org/10.1016/j.bcmd.2011.04.001>.
75. Lino, A.C., Dang, V.D., Lampropoulou, V., Welle, A., Joedicke, J., Pohar, J., Simon, Q., Thalmensi, J., Baures, A., Flüher, V., et al. (2018). LAG-3 inhibitory receptor expression identifies immunosuppressive natural regulatory plasma cells. *Immunity* 49, 120–133.e9. <https://doi.org/10.1016/j.immuni.2018.06.007>.
76. Levine-Tiefenbrun, M., Yelin, I., Katz, R., Herzel, E., Golan, Z., Schreiber, L., Wolf, T., Nadler, V., Ben-Tov, A., Kuint, J., et al. (2021). Initial report of decreased SARS-CoV-2 viral load after inoculation with the BNT162b2 vaccine. *Nat. Med.* 27, 790–792. <https://doi.org/10.1038/s41591-021-01316-7>.
77. Sielaff, M., Kuharev, J., Bohn, T., Hahlbrock, J., Bopp, T., Tenzer, S., and Distler, U. (2017). Evaluation of FASP, SP3, and iST protocols for proteomic sample preparation in the low microgram range. *J. Proteome Res.* 16, 4060–4072. <https://doi.org/10.1021/acs.jproteome.7b00433>.
78. Meier, F., Brunner, A.D., Frank, M., Ha, A., Bludau, I., Voytik, E., Kaspar-Schoenefeld, S., Lubeck, M., Raether, O., Bache, N., et al. (2020). diaPASEF: parallel accumulation-serial fragmentation combined with data-independent acquisition. *Nat. Methods* 17, 1229–1236. <https://doi.org/10.1038/s41592-020-00998-0>.
79. Demichev, V., Messner, C.B., Vernardis, S.I., Lilley, K.S., and Ralser, M. (2020). DIA-NN: neural networks and interference correction enable deep proteome coverage in high throughput. *Nat. Methods* 17, 41–44. <https://doi.org/10.1038/s41592-019-0638-x>.
80. UniProt Consortium (2021). UniProt: the universal protein knowledgebase in 2021. *Nucleic Acids Res.* 49, D480–D489. <https://doi.org/10.1093/nar/gkaa1100>.
81. R-Core-Team. (2021). R: A Language and Environment for Statistical Computing (Vienna, Austria: R Foundation for Statistical Computing). URL: <https://www.R-project.org/>.
82. Wickham, H., Averick, M., Bryan, J., Chang, W., McGowan, L., François, R., Grolemund, G., Hayes, A., Henry, L., Hester, J., et al. (2019). Welcome to the tidyverse. *J. Open Source Softw.* 4, 1686.
83. Szklarczyk, D., Gable, A.L., Nastou, K.C., Lyon, D., Kirsch, R., Pyysalo, S., Doncheva, N.T., Legeay, M., Fang, T., Bork, P., et al. (2021). The STRING database in 2021: customizable protein-protein networks, and functional characterization of user-uploaded gene/measurement sets. *Nucleic Acids Res.* 49, D605–D612. <https://doi.org/10.1093/nar/gkaa1074>.
84. Ritchie, M.E., Phipson, B., Wu, D., Hu, Y., Law, C.W., Shi, W., and Smyth, G.K. (2015). Limma powers differential expression analyses for RNA-sequencing and microarray studies. *Nucleic Acids Res.* 43, e47. <https://doi.org/10.1093/nar/gkv007>.

STAR★METHODS

KEY RESOURCES TABLE

REAGENT or RESOURCE	SOURCE	IDENTIFIER
<b>Antibodies</b>		
Anti-mouse Fas (clone Jo2)	BD Bioscience	Cat: #5654258; RRID:N/A
Anti-mouse CD19 (clone 6D5)	eBioscience	Cat. #115520; RRID:AB_313655
Anti-mouse B220 (clone RA3-6B2)	Biolegend	Cat. #103234; RRID:AB_893353
Anti-mouse IgM (clone II/41)	eBioscience	Cat. #25–5790; RRID:AB_469655
Anti-mouse IgD (clone 11–26)	eBioscience	Cat. #48–5993; RRID:AB_1272239
Anti-mouse CD1d (clone 1B1)	BioLegend	Cat. #123514; RRID: AB_2073523
Anti-mouse CD5 (clone 53–7.3)	Biolegend	Cat. #100626; RRID:AB_2563929
Anti-mouse CD21/CD35 (clone 7E9)	BioLegend	Cat. #123414; RRID: AB_2085158
Anti-mouse CD23 (clone B3B4)	BioLegend	Cat. #101620; RRID: AB_2563439
Anti-mouse CD38 (clone 90)	eBioscience	Cat. #17–0381; RRID: AB_469382
Anti-mouse CD43 (clone S7)	BD Bioscience	Cat. #553269; RRID:AB_2255226
Anti-mouse CD90.2 (clone 53–2.1)	eBioscience	Cat. #140310; RRID:AB_10643586
Anti-mouse CD19 (clone 6D5)	BioLegend	Cat. #115530; RRID: AB_830707
Anti-mouse CCR1 (clone S15040E)	BioLegend	Cat. #152508; RRID: AB_2800689
Anti-mouse CCR7 (clone 4B12)	BioLegend	Cat. #120106; RRID: AB_389358
Anti-mouse CXCR4 (clone L276F12)	BioLegend	Cat. #146506; RRID: AB_2562783
Anti-mouse CD131 (clone JORO50)	BD Biosciences	Cat. #559920; RRID: AB_397374
Anti-mouse CD148 (clone 8A-1)	BD Biosciences	Cat. #565747; RRID:AB_2664391
Anti-mouse CD200 (clone OX-90)	BioLegend	Cat. #123808; RRID:AB_2073942
Anti-mouse CD267 (TACI; clone 8F10)	BioLegend	Cat. #133403 RRID: AB_2203542
Anti-mouse CD138 (clone 281-2)	BioLegend	Cat. #142507 RRID: AB_11204257
Anti-mouse Lair1	Abcam	Cat. #ab95749; RRID: AB_10679232
Anti-human CD20 (clone L27)	BD Biosciences	Cat. #335828; RRID:AB_2868689
Anti-human CD27 (clone L128)	BD Biosciences	Cat. #337169; RRID:AB_647368
Anti-human IgD (clone IA6-2)	BD Biosciences	Cat. #740794; RRID:AB_2740457
Anti-human IgA-Biot (clone G20-359)	BD Biosciences	Cat. #555884; RRID:AB_396196
Anti-human IgG-Biot (clone G18-145)	BD Biosciences	Cat. #555785; RRID:AB_396120
Anti-human IgE-Biot (clone G7-26)	BD Biosciences	Cat. #555858; RRID:AB_396180
Anti-human CD27-Biot (clone M-T271)	BD Biosciences	Cat. #356426; RRID:AB_2571912
Anti-human CCR1 (clone 5F10B29)	BioLegend	Cat. #362903; RRID:AB_2563897
Anti-human CCR7 (clone G043H7)	BioLegend	Cat. # 53203; RRID:AB_10916391
Anti-human CXCR4 (clone 12G5)	BioLegend	Cat. #306505; RRID:AB_314611
Anti-human CD131 (clone 1C1)	BioLegend	Cat. #306104; RRID:AB_2085808
Anti-human CD148 (clone A3)	BioLegend	Cat. #328708; RRID:AB_2174826
Anti-human CD200 (clone OX-104)	BioLegend	Cat. #329205; RRID:AB_1027677
Anti-human Lair1 (clone NKTA255)	BioLegend	Cat. #342801; RRID:AB_1659239
Anti-human Foxo1 (clone C29H4)	Cell Signaling	Cat. #72874S; RRID: AB_2799829
Anti-mouse IgM	SouthernBiotech Associates	Cat. #1020-08; RRID: AB_2737411
Anti-mouse IgG1	SouthernBiotech Associates	Cat. #1070-08; RRID: AB_2794413
p-Akt Ser473	Cell Signaling	Cat. #9271; RRID: AB_329825
p-Akt Thr308	Cell Signaling	Cat. #9275; RRID: AB_329828
p-Tyr	Santa Cruz	Cat. #sc-7020; RRID: AB_628123
β-Actin	Santa Cruz	Cat. #sc-47778; RRID: AB_2714189

(Continued on next page)

**Continued**

REAGENT or RESOURCE	SOURCE	IDENTIFIER
β-Actin	Sigma Aldrich	Cat- #A3854; RRID: AB_262011
Notch2	Cell Signaling	Cat. #5732S; RRID: AB_10693319
Akt (pan)	Cell Signaling	Cat. #2920; RRID: AB_1147620
p-Btk (Tyr223)	Cell Signaling	Cat. #87141; RRID: AB_2800099
Btk (C82B8)	Cell Signaling	Cat. #3533; RRID: AB_2067811
pS6 Ser235/236	Cell Signaling	Cat. #3945; RRID: AB_2146236
pPLCγ2 Tyr759	Cell Signaling	Cat. #3874; RRID: AB_2163714
CD19	Cell Signaling	Cat #90176; RRID: AB_2800152
GAPDH (D16H11)	Cell Signaling	Cat #5174; RRID: AB_10622025
p-CD19 Tyr500	Thermo Fisher	Cat. #PA5-118772; RRID: AB_2903272
p-CD79a Tyr199	Thermo Fisher	Cat. #PA5-105487; RRID: AB_2816915
p-Syk (Tyr525/526)	Thermo Fisher	Cat #MA5-14918; RRID: AB_10989513
Syk	Thermo Fisher	Cat #PA5-27262; RRID: AB_2544738
MOMA-1	BMA Biomedicals	Cat. #T-2011; RRID: AB_1227422
CD1d	Biologend	Cat. #123506; RRID: AB_1236548
CD45R/B220	ThermoFisher	Cat #14-0452-82; RRID: AB_467254
CD3 (17A2)	ThermoFisher	Cat #14-0032-82; RRID: AB_467053
Chemicals		
Amersham ECL PLUS Western Blotting Detection Reagents	GE Healthcare UK	Cat. #10001486
Violet Cell Trace	Invitrogen	Cat. #C34557
Fixable Viability Dye APC-efl780	eBioscience	Cat. #65-0865
Fixable Viability Dye V450	eBioscience	Cat. #65-0863
Fixable Viability Dye efl506	eBioscience	Cat. #65-0866
Anti-mouse PNA	Sigma Aldrich	Cat. #L6135
NP-CGG	Biosearch Technologies	Cat. #N-5055C-5
CpG-C DNA	Hycultec	Cat. #HC-4041
Fluo-4, AM	Thermo Scientific	Cat. #F14201
ALP (Substrate for AP)	Roche	Cat. #12172933
Streptavidin-A P-conjugate	Thermo Scientific	Cat. #11089161001
NP-LPS	LGC Biosearch Technologies	Cat. #N-5065-1
NP-BSA	LGC Biosearch Technologies	Cat. #N-5050M
Inject Alum	Thermo Scientific	Cat. #77161
Fura Red™, AM	Thermo Scientific	Cat. #F3021
Biological samples		
Human Spleen samples	Necker Hospital, Paris Henry Mondor Hospital, Créteil	N/A
Chemicals, peptides, and recombinant proteins		
MK-2206 AKT inhibitor	AbMole Bioscience	Cat. #M1837
MitoTracker™ Green FM	Thermo Fisher Scientific	Cat. #M7514
DAPI	Sigma	Cat. #D8417
Propidium Iodide	Sigma	Cat. #P4864
2-Mercaptoethanol	Life Technologies	Cat. #31350010
Trypsin 0.5% EDTA	Life Technologies	Cat. #25300054
Critical commercial assays		
Gene Chip Mouse 430 2.0	Affymetrix GmbH	Cat. #900495
Bio-Plex Pro Mouse Cytokine IL-10 Set, 1 3 96 well	Bio-Rad	Cat. #171-G5009M
Bio-Plex Pro Mouse Cytokine IL-6 Set, 1 3 96 well	Bio-Rad	Cat. #171-G5007M

(Continued on next page)

**Continued**

REAGENT or RESOURCE	SOURCE	IDENTIFIER
<b>Deposited data</b>		
Raw and analyzed human array data	This paper	E-MTAB-2246, E-MTAB-9620
Raw and analyzed mouse array data	This paper	GSE164765
Phospho-proteomics data	This paper	PXD031433
<b>Experimental models: Cell lines</b>		
Mouse: OP9-hDLL1 cells	Six et al. <sup>74</sup>	N/A
Human: REC-1 cells	ATCC	CRL-3004
<b>Experimental models: Organisms/strains</b>		
Mouse: R26-fl-Akt-C	PMID: 33140819	N/A
Mouse: R26-fl-FoxO1ADA	PMID: 22057897	N/A
Mouse: CD19-Cre	PMID: 7543183	N/A
<b>Software and algorithms</b>		
FLOWJO X 10.0.7	<a href="https://www.flowjo.com/solutions/flowjo/">https://www.flowjo.com/solutions/flowjo/</a>	RRID: SCR_008520
GraphPad Prism 8	<a href="https://www.graphpad.com/scientific-software/prism/">https://www.graphpad.com/scientific-software/prism/</a>	RRID: SCR_002798
<b>Other</b>		
Lipopolysaccharides from <i>Escherichia coli</i> 055:B5	Sigma	Cat. #L2637-25MG
Penicillin/Streptomycin sol	Life Technologies	Cat. #15140-122
DMEM	Life Technologies	Cat. #61965026
FBS South America	BIOWEST	Cat. #S1810-500
Bovine Serum Albumin	Sigma-Aldrich	Cat. #A7906-100G
Fixation/Permeabilization Solution Kit	BD Bioscience	Cat# 554714

**RESOURCE AVAILABILITY**

**Lead contact**

Further information and requests for resources and reagents should be directed to and will be fulfilled by the lead contact Nadine Hövelmeyer [hoevelme@uni-mainz.de](mailto:hoevelme@uni-mainz.de).

**Materials availability**

Certain materials are shared with academic and non-profit research organizations for research and educational purposes only under an MTA to be discussed in good faith with the recipient.

**Data and code availability**

- Mouse Affymetrix gene array data have been deposited at NCBI GEO depository and are accessible with the accession number GSE164765, or using the link <https://www.ncbi.nlm.nih.gov/geo/query/acc.cgi?acc=GSE164765>. Human Affymetrix data have been deposited at [www.ebi.ac.uk/arrayexpress](http://www.ebi.ac.uk/arrayexpress) with accession numbers E-MTAB-2246 (IgD<sup>+</sup>CD27<sup>+</sup>, IgD<sup>-</sup>CD27<sup>+</sup>) and E-MTAB-9620 (IgD<sup>+</sup>CD27<sup>-</sup>). Phospho-proteomics: All raw files, processing outputs and log files as well as R scripts for processing and their respective outputs are available at <http://www.proteomexchange.org> with repository identifier PXD031433.
- This paper does not report original code.
- Any additional information required to reanalyze the data reported in this paper is available from the **lead contact** upon request.

**EXPERIMENTAL MODEL AND SUBJECT DETAILS**

**Mice**

AKT-C<sup>35</sup> and FoxO1<sup>ADA49</sup> mice were generated as previously described and kindly provided by F.Thomas Wunderlich (MPI, Cologne). B-cell specific AKT-overexpressing mice were generated by crossing AKT<sup>1<sup>fl/stop</sup></sup> with *Cd19-cre* mice<sup>22</sup> (AKT<sup>+/-</sup> *Cd19-cre*<sup>+/-</sup> = AKT<sup>BOE</sup>). B cells from AKT<sup>BOE</sup> and *Cd19-cre* FoxO1<sup>ADA</sup> mice were pre-gated on eGFP<sup>+</sup> B cells. Heterozygous Cre recombinase mice were used in all experiments unless otherwise stated. Mice were of C57BL/6J strain, 8–12-week-old at start of experiments, unless otherwise stated, and of sex-matched male and female genders. All experiments were in accordance with

the guidelines of the Translational Animal Research Center (TARC) of the University of Mainz and approved by the institutional committee on animal experimentation and the government of Rheinland-Pfalz (RLP). All experiments were reviewed and approved by appropriate institutional review committees (LAGeSo Berlin), and were conducted according to French, and German legislations, in compliance with European community council directive 68/609/EEC guidelines.

### Human samples

This study was conducted in accordance with the Declaration of Helsinki, with informed consent from each patient or the patient's family. Splens were obtained from patients undergoing a splenectomy for nonimmunological disease-related reasons (spherocytosis or sickle cell anemia). The transcriptome of CD27<sup>-</sup>IgD<sup>+</sup> splenic B cells corresponds to paired samples from previously published CD27<sup>+</sup>IgD<sup>+</sup> samples.<sup>15</sup> Splens were also obtained from organ donors. This study was authorized by the French Agence Nationale de la Biomédecine. Human splens analyzed by flow cytometry were from female and male organ donors, age between 32 and 64 years old. Human splens used to isolate marginal zone B cell precursors (MZP) were from female and male donors undergoing splenectomy for nonimmunological disease-related reasons, age between 6 and 12 years old. Human ALPS blood samples and their controls were from male and female donors, age between 3 and 34 years old.

## METHOD DETAILS

### Cell sorting of MZP and *in vitro* differentiation assay

To isolate MZP cells, naive B cells were first enriched from total spleen mononuclear cells by negative selection with the Naive B Cell Isolation Kit II and AutoMACS Pro (Miltenyi Biotec). Untouched naive B cells were then cultured at 37°C in RPMI 10% FCS at 10<sup>7</sup> cells/mL and pulsed with MitoTracker Green (MTG; Thermo fisher) at 10 μM during 30 min. After three washes, cells were chased for 1 h at 37°C and were then stained on ice for 15 min with the following Abs: anti-IgG-biotin, -IgA-biotin, -IgE-biotin, -CD27-biotin, -CD20-PECy7, -CD45RB-PE. After three washes, cells were incubated with Streptavidin-Brilliant violet (BV) 785 during 15 min and washed three times. MZP cells were defined as Streptavidin-BV785<sup>neg</sup>CD20<sup>+</sup>MTG<sup>neg</sup>CD45RB<sup>+</sup> and isolated on FACSria Cell Sorter (BD Biosciences).

The influence of AKT signaling on the differentiation of MZP cells into MZ-like B cells was tested by plating them on mouse OP9 stromal cells engineered to express either the GFP alone (OP9) or GFP and the human Notch ligand Delta-like1 gene (OP9-hDLL1; gift from Emmanuelle Six, Institut Imagine, Paris, France).<sup>74</sup> The day before MZP cell sorting, OP9 and OP9-hDLL1 cells were plated in 48-well plates at 20,000 cells/well in MEM alpha medium (Thermo fisher) containing 20% FCS and 1% Pen-Strep (Thermo fisher). Sorted MZP were added on OP9 or OP9-hDLL1 (50,000 cells per well) and cultured in the presence of the AKT inhibitor MK-2206 (200 nM; AbMole Bioscience) or DMSO. After three days, cells were washed, stained with viability dye, anti-CD20, -IgD, -CD148, and -CD27 antibodies, and lymphoid CD20<sup>+</sup>GFP<sup>neg</sup> cells were analyzed by flow cytometry for the expression of CD27 and CD148.

### Mouse cell purification and *in vitro* assays

Total B cells were purified from erythrocyte-lysed single-cell suspensions of splenocytes by selection with anti-CD19 or anti-CD43 microbeads using the B cells Isolation Kit (Miltenyi Biotec), according to the manufacturer's instruction. Reached purity from 95 to 98% was evaluated by flow cytometry.

To assess cell division, B cells were labeled with CellTrace<sup>TM</sup> Violet - Cell Proliferation Kit (Invitrogen, Paisley, UK). Purified B cells were resuspended in 1 mL 37°C warm PBS per 10<sup>6</sup> cells and 5 μM CellTrace (5 mM stock in DMSO, Molecular probes) and incubated in the dark for 20 min at RT. The reaction was stopped by addition of 10 mL DMEM supplemented with 10% fetal calf serum (FCS), 1% Penicillin (10,000 Units/mL), and Streptomycin (10,000 μg/mL), 1% L-glutamine (200 mM), 1% nonessential amino acids (100×), 1% sodium pyruvate (100×), 1% *N*-2-hydroxyethylpiperazine-*N*-2-ethanesulfonic acid (HEPES) (1 M), and 50 μM β-mercaptoethanol. Triplicates of 300,000 labeled cells were plated in a 96-well round bottom plates. Cells were incubated in media, and media supplemented with 50 ng/mL BAFF (R&D systems), 10 μg/mL anti-IgM (Jackson ImmunoResearch), 20 μg/mL LPS (Sigma-Aldrich), 10 μg/mL anti-CD40 (R&D System, Wiesbaden, Germany), or 0.1 μM CpG (InvivoGen) and incubated at 37°C, 5% CO<sub>2</sub>. Labeled cells were analyzed by flow cytometry after four days.

For cytokine production analysis, B cell subsets were stimulated at 5 × 10<sup>5</sup> cells per well in 96-well flat in complete RPMI or with LPS (1 μg/mL) and agonistic anti-CD40 antibody (clone FGK-45, produced at DRFZ at 10 μg/mL). After 24 h, 150 μL supernatant of activated cells was collected and transferred into new 96 well plates and kept at -20°C until further use. 50 μL of supernatant was used to measure cytokine concentration using Bio-Plex kits (Bio-Rad) according to the manufacturer's instruction.

To assess B cell survival, splenic B cells purified by depletion of CD43<sup>+</sup> cells by MACS (Miltenyi) were cultured seeding 2 × 10<sup>6</sup> cells in 1 mL of complete RPMI medium and live B cells were counted daily.

For plasmablast-differentiation assays cells were cultured at a density of 5 × 10<sup>5</sup> cells/mL in flat-bottom 96 well plates. Cells were harvested after 48 h and analyzed by flow cytometry after staining with anti-B220 and anti-CD138 antibodies. Dead cells were discriminated from living cells using a fixable dead cell staining kit (Invitrogen).

For transcriptome analyses, B cells obtained using anti-CD43 microbeads were treated with FcγR block, and cell suspensions were stained with anti-CD19, -CD21, -CD23, -CD1d, and cells were sorted as Dapi-negative, CD19<sup>+</sup> and CD1d<sup>low</sup>CD23<sup>+</sup>CD21<sup>+</sup> (FO), and CD1d<sup>high</sup>CD23<sup>-</sup>CD21<sup>high</sup> (MZ).

### Flow cytometry

Flow cytometric staining was performed as previously described.<sup>75</sup> For surface staining cells were blocked with anti-CD16/32 (clone 2.4G2, BD Bioscience) and stained with the indicated combination of fluorochrome-conjugated antibodies for 20 min on ice. For biotinylated antibodies, cells were further incubated with Streptavidin conjugated to fluorochrome for 15 min. Dead cells were excluded by DAPI or PI, and fixable Viability Dyes (eBioscience, Cat. # 65–0865, 65–0863, 65–0866). All cells were acquired on BD FACS Canto II, Fortessa flow cytometers and analyzed with FlowJo software (version 8.87). For ImageStream analysis, human splenic samples were stained as described above and permeabilized with Fix & Perm reagents (Caltag Laboratories) for FOXO1 staining. Samples were run on an ImageStream X Mk II (Amnis Corp, Luminex) and a 60x magnification was used for all acquisitions. Data were acquired using the INSPIRE software (Amnis Corp, Luminex) and analyzed using the IDEAS software (version 6.2 Amnis Corp, Luminex). At least, 30,000 events were collected for each B cell subpopulation in all experiments.

### Immunization and ELISA

To measure T cell-T-independent<sup>76</sup> immune responses, age-matched AKT<sup>BOE</sup> and control mice were immunized intraperitoneally (i.p.) with 10  $\mu$ g/mouse NP<sub>27</sub>-Ficoll (Biosearch Technologies) or with 10  $\mu$ g/mouse NP-LPS (LGC Biosearch) in 200  $\mu$ L sterile PBS. To measure T-cell-dependent response, age-matched mice were immunized with 20  $\mu$ g alum-precipitated NP<sub>28</sub>-CGG (Biosearch Technologies). Serum was taken from tail vein on day 0 (unimmunized), 7, 14, 21, and 28 after immunization. Antibody titers and NP-specific antibodies were determined by ELISA using NP-specific standards.

### Western blot analysis

Extract preparation and Western blot analysis were performed as previously described.<sup>3</sup> Membranes were then incubated for 1h at RT with secondary HRP conjugated donkey- $\alpha$ -rabbit or goat- $\alpha$ -mouse antibodies in 5% (w/v) NF-milk/TBS/0.01% Tween, except for Actin (SantaCruz), which is directly HRP conjugated, was dissolved in NF-milk/TBS/0.01% Tween and the membranes were incubated for 1h at RT. Amersham<sup>TM</sup> ECL Prime Western blotting reagent (GE Healthcare Life Science) was used as a substrate for the HRP reaction and exposed in Molecular Imager Gel Doc<sup>TM</sup> XR System (Bio-Rad Laboratories GmbH). Primary antibodies used: anti-p-Akt<sup>Ser473</sup>, -p-Akt<sup>Thr308</sup>, -Akt, -Notch2 (Cell Signaling), p-Tyr (Santa Cruz).

### Immunohistochemistry

Spleen tissue samples were embedded in Tissue-TEK OCT compound (Sakura Finetek) and frozen at  $-80^{\circ}\text{C}$ . For immunofluorescence staining, 8 $\mu$ m sections were thawed, air dried, fixed with 4% paraformaldehyde and stained with primary antibody overnight at 4 $^{\circ}\text{C}$  in a humidified chamber. Used antibodies:  $\alpha$ -B220 (BD Pharmingen),  $\alpha$ -CD1d (eBioscience),  $\alpha$ -CD3 (BD), and  $\alpha$ -MOMA-1 (eBioscience). Slides were incubated for 30 min at room temperature with a biotinylated secondary antibody (Dianova). Finally, slides were treated with streptavidin-HRP and stained with Tyramide (Cy3) and Fluorescein (FITC) according to the manufacturer's instructions (PerkinElmer). Slides were covered with Mounting Medium with DAPI (Vector H-1200, Vector Laboratories). Sections were examined using a Leica AF6000X fluorescence microscope, and images were acquired with a Hamamatsu video camera and processed with Imaris software.

### Measurement of intracellular calcium flux

Calcium flux was measured using FuraRed (PerCP) and Fluo-4 (FITC) (Invitrogen by life technologies). The fluorescence intensity of FuraRed decreases with the uptake of  $\text{Ca}^{2+}$ . For Fluo-4, the fluorescence intensity goes up with the  $\text{Ca}^{2+}$ -binding. The FACS Canto II (BD Biosciences) was used to measure the fluorescence.  $10 \times 10^6$  CD19 MACS purified B cells were stained and afterward  $4 \times 10^6$  B cells were used for the measurement. Sit flush was shut down at the FACSCanto II to measure  $\text{Ca}^{2+}$  flux before the reaction was completed. First, the baseline of the B cells was recorded for 1min. Measurement was paused and 5 $\mu$ g/mL  $\alpha$ IgM added to the cells to activate them and trigger the  $\text{Ca}^{2+}$  release. Cells were immediately measured for 4min after  $\alpha$ IgM addition. As a positive control, 5 $\mu$ M Ionomycin was added to trigger a  $\text{Ca}^{2+}$  release and measured for 1 min; as a negative control, 10mM EGTA was used for the uptake of  $\text{Ca}^{2+}$  and measured for 2min. Since efficiency of dye uptake differ from cell to cell, the intensity of only one dye cannot be used for comparison. Therefore, for the analysis the ratio between the fluorescence intensities of the two chelating-antibodies was calculated.

### Proteomics sample preparation

Pellets of B cells isolated from 16 mice (wild type and AKT overexpression mice +/- stimulation with anti-IgM for 15 min, four biological replicates each) were prepared for proteome and phosphoproteome analysis. The cells were lysed in an urea-containing buffer (7 M Urea, 2 M Thiourea, 1% Sigma Aldrich Phosphatase Inhibitor Cocktail 3 in 100 mM  $\text{NH}_4\text{HCO}_3$ ) by sonication for 15 min (30 s on/off cycles) at 4 $^{\circ}\text{C}$  with high power in a Bioruptor device (Diagenode, Liège, Belgium). After centrifugation for 15 min at 4 $^{\circ}\text{C}$ , the protein concentration of the supernatant was determined using the Pierce 660 nm protein assay (Thermo Fisher Scientific, Waltham, MA, USA) according to the manufacturer's protocol. 250 $\mu$ g of protein were digested in 25  $\mu$ g aliquots following the filter aided sample preparation protocol as previously described.<sup>77</sup> After digest, a peptide aliquot corresponding to 10  $\mu$ g of protein was lyophilized and reconstituted in 40  $\mu$ L 0.1% formic acid (FA) for whole proteome analysis. 200  $\mu$ g of the remaining peptides were subjected to phosphopeptide enrichment using magnetic Zr-IMAC HP beads (ReSyn Biosciences, Edenvale, South Africa) following the manufacturer's protocol. The purified phosphopeptides were desalted using SepPak tC18  $\mu$ Elution plate (Waters, Milford, MA, USA), lyophilized and reconstituted in 20  $\mu$ L 0.1% FA.

### Liquid-chromatography mass spectrometry (LC-MS)

For the LC-MS analysis of the full proteome, 100 ng of the reconstituted peptides were separated on a nanoElute LC system (Bruker Corporation, Billerica, MA, USA) at 400 nL/min using a reversed phase C18 column (Aurora UHPLC emitter column, 25 cm × 75 μm 1.6 μm, IonOpticks) which was heated to 50°C. Peptides were loaded onto the column in direct injection mode at 600 bar. Mobile phase A was 0.1% FA (v/v) in water and mobile phase B 0.1% FA (v/v) in ACN. Peptides were separated running a linear gradient from 2% to 37% mobile phase B over 39 min. Afterward, column was rinsed for 5 min at 95% B. Eluting peptides were analyzed in positive mode ESI-MS using parallel accumulation serial fragmentation (PASEF) enhanced data-independent acquisition mode (DIA) on a timsTOF Pro 2 mass spectrometer (Bruker Corporation).<sup>78</sup> The dual TIMS (trapped ion mobility spectrometer) was operated at a fixed duty cycle close to 100% using equal accumulation and ramp times of 100 m each spanning a mobility range from  $1/K_0 = 0.6 \text{ Vs. cm}^{-2}$  to  $1.6 \text{ Vs. cm}^{-2}$ . We defined  $36 \times 25$  Th isolation windows from  $m/z$  300 to 1,165 resulting in fifteen diaPASEF scans per acquisition cycle. The collision energy was ramped linearly as a function of the mobility from 59 eV at  $1/K_0 = 1.3 \text{ Vs. cm}^{-2}$  to 20 eV at  $1/K_0 = 0.85 \text{ Vs. cm}^{-2}$ . All samples were measured in triplicates.

To characterize the phosphoproteome, 3 μL of the reconstituted phosphopeptides were separated on a nanoElute LC system (Bruker Corporation, Billerica, MA, USA) at 400 nL/min using a reversed phase C18 column (Aurora UHPLC emitter column, 25 cm × 75 μm 1.6 μm, IonOpticks) which was heated to 50°C. Peptides were loaded onto the column in direct injection mode at 600 bar. Mobile phase A was 0.1% FA (v/v) in water and mobile phase B 0.1% FA (v/v) in ACN. Peptides were separated running a linear gradient from 2% to 37% mobile phase B over 39 min. Afterward, column was rinsed for 5 min at 95% B. Eluting peptides were analyzed in positive mode ESI-MS using parallel accumulation serial fragmentation (PASEF) enhanced data-independent acquisition mode (DIA) on a timsTOF SCP mass spectrometer (Bruker Corporation).<sup>78</sup> The dual TIMS was operated at a fixed duty cycle close to 100% using equal accumulation and ramp times of 166 m each spanning a mobility range from  $1/K_0 = 0.7 \text{ Vs. cm}^{-2}$  to  $1.3 \text{ Vs. cm}^{-2}$ . We defined  $29 \times 25$  Th isolation windows from  $m/z$  280 to 990 resulting in ten diaPASEF scans per acquisition cycle. The collision energy was ramped linearly as a function of the mobility from 59 eV at  $1/K_0 = 1.6 \text{ Vs. cm}^{-2}$  to 20 eV at  $1/K_0 = 0.6 \text{ Vs. cm}^{-2}$ . All samples were measured in triplicates.

### Raw data processing

Peptides were identified and label-free quantification (LFQ) of proteins was performed using DIA-NN (v1.8).<sup>79</sup> Full proteome samples were processed using library free mode with standard parameters, except for tryptic cleavage sites considering no cleavage before proline. The FASTA protein database contained 17,090 reviewed (Swissprot) protein entries of the mouse reference proteome and 172 common contaminant proteins and was obtained on 25<sup>th</sup> November 2021 from [uniprot.org](http://uniprot.org).<sup>80</sup> Phosphopeptide samples were processed using a predicted library from DIA-NN based on a FASTA protein database containing 17,082 reviewed (Swissprot) protein entries of the mouse reference proteome and 172 common contaminant proteins and was obtained on 9<sup>th</sup> November 2021 from [uniprot.org](http://uniprot.org).<sup>80</sup> For precursor and fragment ion prediction, the precursor charge range was set between 1 and 4 and the range for fragment ions and precursor mass to charge ratio was limited to 250–1250  $m/z$ . The peptide length was set to 7–30. Tryptic cleavage considering no cleavage after the lysine or arginine is followed by proline, maximum one missed cleavage was allowed. *N*-terminal methionine excision was enabled and cysteine carbamidomethylation was set as fixed modification. The maximum number of variable modifications was set to 3, allowing only UniMod:21 modifications, i.e., mass delta of 79.9663 corresponding to phosphorylation at serine, threonine and tyrosine. The prediction resulted in a spectral library including 30,274,157 precursors. The standard processing parameters of DIA-NN were used for the library search, except enabling low RAM usage option.

The resulting peptide and protein quantification LC-MS results were further analyzed using the statistical programming language R, including the tidyverse package.<sup>81,82</sup> Fold changes (FC) were calculated using median intensity values. Two-side t test assuming equal variances was performed for all samples that could be confidently identified with valid intensity values in at least 60%. All samples that were confidently appearing or disappearing in AKT overexpression mice (i.e., at least 60% identified intensities in one of the groups and only NAs in the other group) were assigned an arbitrary FC of 100 and 0.01 as well as an arbitrary p value of 0.001. The resulting p values were corrected for multiple testing using the Benjamini-Hochberg (FDR) method. The resulting proteins and phosphopeptides were then filtered for FCs >2 and <0.5 and an adjusted p value of <0.05. All significantly changing phosphoproteins were submitted to gene ontology enrichment analysis using STRING-DB.<sup>83</sup>

### Microarray and statistical analysis

The significantly differentially regulated genes were detected using limma R package<sup>84</sup> after signal normalization obtained with gcrma R package (Jean Wu and Rafael Irizarry with contributions from James MacDonald Jeff Gentry (2020). gcrma: Background Adjustment Using Sequence Information. R package version 2.60.0), with p values adjusted using Benjamini Hochberg procedure. In order to be selected in a comparison of two conditions, each Affy IDs had to fulfill the following criteria: (i) be present in at least two of the three arrays for at least one of the two conditions compared, (ii) to have a mean signal intensity higher than 50 in at least one of the two conditions, and (iii) to show an adjusted p value <0.01 (limma) in the comparison of the two conditions. Transcriptional regulators and transmembrane receptors were extracted using the gene ontology resource ([www.geneontology.org](http://www.geneontology.org)).<sup>75</sup> Human microarray data were processed as described previously to capture genes with  $p < 0.05$ , and at least a 1.5-fold expression difference between samples.<sup>15</sup> Heat-maps were produced using pheatmap R package (Raivo Kolde (2015). pheatmap: Pretty Heatmaps. R package version 1.0.2. <http://CRAN.R-project.org/package=pheatmap>).

### Gene array hybridization

cRNA were hybridized on Affymetrix MG 430 2.0 arrays using standard Affymetrix protocol after quality control with Agilent 2100 Bioanalyzer and quantification with NanoDrop ND-1000 spectrophotometer.

### QUANTIFICATION AND STATISTICAL ANALYSIS

Prism 8 software (GraphPad) was used for data analysis. We observed normal distribution. Comparison of two groups were calculated using unpaired two-tailed Student's *t* test for parametric and Mann-Whitney test or Wilcoxon test for nonparametric distributions. Multiple comparison was corrected for using the Holm-Šidák method. For comparison of more than two groups, one-way ANOVA with Bonferroni's posthoc test or Kruskal-Wallis test was used. Data are represented as means  $\pm$  SEM or mean  $\pm$  SD, as indicated. Statistical significance: \**p* value <0.05; \*\**p* value <0.01; \*\*\**p* value <0.001; \*\*\*\**p* < 0.0001). ELISA was analyzed with SoftMax Pro 5.4.1 (Molecular Devices Corporation) and flow cytometry data were analyzed using the FlowJo software 8.87 (FLOWJO, LLC data analysis software). No sample was excluded from analysis.